Palynofacies and geochemical analyses of the Upper Cretaceous–Eocene succession, western Sirte Basin, Libya

El Atfy, H.; Diasty, W. Sh. El; El Beialy, S. Y. ; Gheith, A. M.; Batten, David; Agha, N. N.

Published in:
Journal of Petroleum Science and Engineering

DOI:
10.1016/j.petrol.2017.07.021

Publication date:
2017

Citation for published version (APA):
El Atfy, H., Diasty, W. S. E., El Beialy, S. Y., Gheith, A. M., Batten, D., & Agha, N. N. (2017). Palynofacies and geochemical analyses of the Upper Cretaceous–Eocene succession, western Sirte Basin, Libya: Palaeoenvironmental interpretation and implications for hydrocarbon generation potential. *Journal of Petroleum Science and Engineering*, *157*, 148-163. https://doi.org/10.1016/j.petrol.2017.07.021

Accepted Manuscript

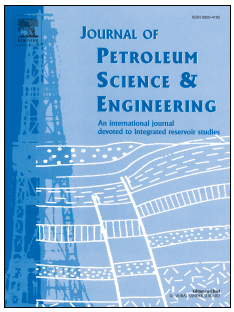

Palynofacies and geochemical analyses of the Upper Cretaceous–Eocene succession, western Sirte Basin, Libya: Palaeoenvironmental interpretation and implications for hydrocarbon generation potential

H. El Atfy, W. Sh El Diasty, S.Y. El Beialy, A.M. Gheith, D.J. Batten, N.N. Agha

PII: S0920-4105(16)30888-9

DOI: 10.1016/j.petrol.2017.07.021

Reference: PETROL 4107

To appear in: *Journal of Petroleum Science and Engineering*

Received Date: 31 October 2016

Revised Date: 5 May 2017

Accepted Date: 10 July 2017

Please cite this article as: El Atfy, H., El Diasty, W.S., El Beialy, S.Y., Gheith, A.M., Batten, D.J., Agha, N.N., Palynofacies and geochemical analyses of the Upper Cretaceous–Eocene succession, western Sirte Basin, Libya: Palaeoenvironmental interpretation and implications for hydrocarbon generation potential, *Journal of Petroleum Science and Engineering* (2017), doi: 10.1016/j.petrol.2017.07.021.

Palynofacies and geochemical analyses of the Upper Cretaceous–Eocene succession, western Sirte Basin, Libya: Palaeoenvironmental interpretation and implications for hydrocarbon generation potential

H. El Atfy[1], W.Sh. El Diasty[1]*, S.Y. El Beialy[1], A.M. Gheith[1], D.J. Batten[2], N.N. Agha[1]

[1] Mansoura University, Faculty of Science, Geology Department, Mansoura 35516, Egypt

[2] Department of Geography and Earth Sciences, Aberystwyth University, Penglais, Aberystwyth SY233DB, and School of Earth, Atmospheric and Environmental Sciences, University of Manchester, Oxford Road, Manchester M13 9PL, UK

* Corresponding author, Dr. Waleed El Diasty, awaleed@mans.edu.eg, Mansoura 35516, (002) 0106 244 3492

Abstract

One hundred and thirty-six core and cuttings samples from Upper Cretaceous–Eocene deposits that are believed to include the most important source rocks in the Sirte Basin have been subjected to Rock-Eval pyrolysis, total organic carbon measurements, and palynofacies and microfacies analyses to determine palaeoenvironments and the thermal maturation history of the succession. It is apparent that the lower part of the Bahi Formation, the oldest rock unit examined, reflects a basin margin environment under the influence of freshwater input. Shallow marine, near-shore, inner shelf, suboxic–anoxic conditions, which are first suggested by the uppermost deposits of the Bahi Formation, prevailed for much of the time during deposition of the younger Cretaceous Etel, Rachmat, Sirte and Kalash formations. Shallow supratidal and intertidal sub-environments alternating with deeper environments of shelf embayments associated with a maximum rise in sea level are indicated by the Paleocene Farrud Member of the Beda Formation. The Zelten Formation consists of shallow intertidal and lagoonal facies, and the overlying Paleocene–Eocene Kheir Formation reflects relatively shallow marine sedimentation in mid to outer shelf environments alternating with short-lived, shallow, intertidal-lagoonal to supratidal conditions. The TOC content of the Upper Cretaceous samples examined is mostly moderate (up to 2.04%), the organic matter consisting of Types II and II/III kerogen. Differences in hydrocarbon generation potential are linked to varying proportions of aquatic versus terrigenous organic matter in the samples examined and hence to depositional conditions. Combined geochemical and palynofacies data reflect deposition mainly in weakly reducing to suboxic settings and suggest that immature to early mature gas-prone source rocks are within the Etel, Rachmat and some of the Sirte Formation, and mature oil/gas-prone source rocks are within the Sirte and Kalash formations.

Key words: Upper Cretaceous–Eocene, palynology, organic facies, organic geochemistry, Concession 11, Sirte Basin, Libya

1. Introduction

The Sirte Basin is the youngest sedimentary basin in Libya (Fig. 1A), one of Africa's most productive petroleum basins, and the world's 13th largest petroleum province. The vast majority of hydrocarbons recovered from Libya have been exploited in this basin, making it of great economic importance and attracting the attention of many exploration geologists and petroleum companies.

The present paper focuses on Concession 11 (Fig. 1A), which is located in the Zallah Trough in the west of the basin (Fig. 1B, C). This concession includes many giant oil fields. In order to improve our understanding of this area and to provide a source rock evaluation of the poorly studied Upper Cretaceous–Eocene successions, sedimentary microfacies, organic geochemical, palynological and palynofacies analyses have been undertaken. Thus, this paper aims to (1) record the different kerogen types and their thermal maturity, (2) determine palaeoenvironmental conditions, (3) define the palynofacies associations of the sedimentary formations studied, and (4) assess the source rock potential for hydrocarbon generation and the role of these units in charging the hydrocarbon reservoirs in the study area.

2. Lithostratigraphy

Abadi et al. (2008) considered the sedimentary succession of the Sirte Basin to consist of three depositional megacycles: pre-rift (Cambro–Ordovician), syn-rift [Upper Cretaceous–Eocene (Ypresian)] and post-rift [Eocene (Lutetian)–Miocene]. The pre- and post-rift deposits are dominated by clastics, whereas the syn-rift (Cretaceous–Eocene) sediments are dominated by non-clastic carbonates and evaporites (Fig. 2). The floor of the basin is delineated by a major unconformity. This is overlain by deposits of the Lower Cretaceous Nubian/Sarir succession, above which is a thick sequence of Upper Cretaceous–Recent sediments. We focus on the syn-rift deposits because of the availability of samples and the economic importance of the succession as a source and reservoir of hydrocarbons in the study area.

The Palaeozoic megacycle begins with the Hofra Formation and ends with the Amal Formation: both are of Cambrian–Ordovician age, overlain unconformably by Lower Cretaceous strata, and underlain by basement where wells have penetrated this in the south-eastern part of the basin. The

cores retrieved consist of metamorphic rocks (chlorite schist and phyllites) and crystalline granites (Fig. 2).

The Cretaceous rocks in the Sirte Basin are divisible into Lower and Upper Cretaceous parts. No samples were available from the so-called Nubian/Sarir Sandstone, so this is not discussed except to note here that the basal Nubian Sandstone consists of a well-defined and widespread stratigraphic unit that is overlain by younger Cretaceous sediments in the western part of the basin (Barr and Weegar, 1972; Abadi et al., 2008).

The first (Upper Cretaceous) depositional cycle consists of the following formations in ascending order: (1) Bahi: a transgressive sequence; (2) Lidam: carbonates, commonly represented by dolomites; (3) Etel: a regressive sequence of carbonates, evaporites and shales; (4) Rachmat: shallow marine deposits resulting from a second transgression; (5) Sirte: deep marine sediments; and (6) Kalash: limestone that accumulated under shallower water conditions.

The Bahi Formation consists of interbedded sandstone, limestone, siltstone and shale and is a significant hydrocarbon reservoir in the Sirte Basin. The sandstones usually consist of medium to coarse, sub-angular to angular quartz grains with a clay matrix (Barr and Weegar, 1972). The formation occurs in the north-western part of the basin and is especially well developed in the Bahi Field area. Its thickness varies from a few metres to a maximum of over 122 m (400 ft: Barr and Weegar, 1972). In the wells studied, LLL1 and AA1, it is 143 m and 122 m thick respectively. Much of the formation appears to be of non-marine origin and may be equivalent to the Nubian Sandstone elsewhere. However, the uppermost few metres of the succession contain glauconite and are probably part of the overlying marine cycle.

The overlying Lidam Formation (Fig. 2) is devoid of fossils (Barr and Weegar, 1972), which means that its age cannot be positively determined. However, it may be constrained by the fact that it occurs at the base of the marine Upper Cretaceous succession and is often overlain by Cenomanian sediments. As no samples were available from the formation, it is not considered further.

The Rakb Group overlies the Lidam Formation and is divided into, from base to top, the Etel, Rachmat and Sirte formations (Fig. 2), which were deposited during a marine transgression. They thicken in the troughs and become thin on, and may be absent from, the platforms (Barr and Weegar, 1972; Hallett, 2002).

The Etel Formation is a sequence of thinly bedded dolomites, anhydrites, shales and siltstones that essentially comprise an alternation of carbonates and evaporites in several of the troughs as a result of Cenomanian–Turonian marine incursions (El-Alami, 1996). A sabkha/lagoonal environment is

indicated with periods of very shallow, near-shore marine deposition and more open marine carbonate accumulation to the north and west. Sea levels were very high and anoxic conditions prevailed. The formation has a sharp contact with the underlying Lidam Formation (Fig. 2), but the junction with the overlying Rachmat Formation is gradational (Fig. 2). It is widely distributed in the south-central part of the basin, but is absent over the platforms. In the QQQ1, LLL1, AA1, FFF1 and GG1 wells it is 378, 299, 137, 360 and 192 m thick, respectively. Fossils are very rare and no age-diagnostic forms have been recognized (Barr and Weegar, 1972). Its age is constrained to Turonian in areas where the formation conformably overlies the Lidam Formation, and is overlain by Coniacian–Santonian beds of the Rachmat Formation (Hallett, 2002).

The Rachmat Formation consists of shales interbedded with minor limestones, sandstones and dolomites. The shales are predominantly grey, fissile to slightly blocky, glauconitic and pyritic in many locations. The dolomites are common in the basal part and characterized by being brown and microcrystalline (Barr and Weegar, 1972; Abadi et al., 2008). The formation contains common foraminifera and ostracodes over much of the basin, which indicate a Coniacian–Santonian age (Barr and Weegar, 1972). It is present in the study area but absent on the platform highs in the basin. It has a maximum thickness of up to 600 m in the Ajdabiya Trough.

The Rachmat Formation is a significant petroleum source rock for the oil fields located along the crest axis of the basement highs of the Sirte Basin. The shale also provides an excellent seal over the Etel Formation (El-Alami, 1996). The thickness of the formation ranges from 207 m in the GG1 well to 128 m in the HHH1 well.

The overlying Sirte Formation (Fig. 2) is considered to be the main source rock in the basin. It is widely distributed throughout the grabens. It consists of a dark-grey to brown shale succession with minor limestone interbeds. Occasionally, the shale is calcareous, silty, sandy and glauconitic or pyritic, with small phosphatic nodules in the lower part of the formation. Deposition was initially in shallow, restricted marine conditions, but subsequently in a rapidly deepening environment (Abadi et al., 2008). The formation has been dated as Campanian on the basis of planktonic foraminifera (Barr and Weegar, 1972). Its average thickness is about 82 m, but it is significantly thicker in the troughs of the basin and thinner on the palaeo-highs (Barr and Weegar, 1972). Thicknesses in the QQQ1, RRR40, AA1, FFF1, GG1 and HHH1 wells considered herein are 253, 152, 875, 149, 378 and 198 m, respectively.

The Kalash Formation, which conformably overlies the Sirte Formation, occurs over most of the Sirte Basin, and delineates the maximum extent of the Cretaceous marine transgression in this region (Abadi et al., 2008). It consists mainly of argillaceous limestone with dark grey calcareous shale

beds in association. The depositional environment indicated is open marine, probably neritic (Barr and Weegar, 1972). The formation is up to 600 m thick in the northern part of the basin and covers both troughs and submerged horsts with relatively little change in facies (Hallett, 2002; Abadi et al., 2008). In the wells studied it is, however, much thinner, ranging from 88 m in the AA1 well to 94 m in the FFF1 well.

The Paleocene deposits of the basin begin with the Danian Hagfa Formation. This is followed upwards by the Selandian Beda Formation and Thanetian Dahra, Zelten and lower Kheir formations. As no samples were available for study from either the Hagfa or the Dahra formations, these are not discussed here.

The Beda Formation consists mainly of various interbedded limestone lithofacies with subordinate dolomite and calcareous shale. It is subdivided into three members from base to top as follows: Thalith, Farrud and Mabruk, of which only the Farrud Member is considered here, samples not being available from the other two. The base of this member consists of carbonate deposits that accumulated during a regression, whereas the upper part comprises fine grained sediments that grade upwards into coarser-grained beds, which were deposited in shallow, agitated water (Barr and Weegar, 1972). The Beda Formation is 259, 357, 238, 387, 260, 262, 250 and 286 m in the QQQ1, LLL1, RRR45, RRR40, RRR1, GG1 and HHH1 wells, respectively.

The Zelten Formation (originally Zelten Limestone) consists of a weakly transgressive sequence of limestone and shale intercalations that have been dated as late Paleocene (Thanetian; Barr and Weegar, 1972). It overlies the Dahra Formation, underlies the Kheir Formation, and is widely distributed in western and central parts of the basin. It forms the principal reservoir of the Zelten Field, and contains lesser reserves in several smaller fields. The thickness on the shelves averages 100–122 m, and in the deeper-water facies reaches up to 137 m (Barr and Weegar, 1972). Its thickness in the QQQ1, RRR1, GG1 and HHH1 wells is 76, 161, 168 and 67 m, respectively.

The Kheir Formation is predominantly shale with some clay, marl and limestone. The shale is grey to dark-grey and green, fissile and calcareous; the clay is grey, soft, and calcareous; the marl is grey, soft and argillaceous; and the limestones are grey calcilutites containing pyrite and many fossils (Barr and Weegar, 1972). In the subsurface the benthic and planktic foraminifera recovered indicate that the formation straddles the Paleocene/Eocene (Thanetian/Ypresian) boundary (Barr and Weegar, 1972). It is 219, 335 and 283 m thick in the QQQ1, AA1 and RRR1 wells, respectively.

3. Structural framework

Tectonically, the Sirte Basin is one of the important structural features in northern Libya. It is heavily fractured with major faults resulting in a number of NW–SE trending grabens (Fig. 1B). These are, from the west to east: Hun, Zallah, Maradah, Ajdabiya and Hameimat. The platforms on the intervening horst blocks in the same direction are: Waddan, Al Bayda, Az Zahrah and Zaltan/Zelten (Ahlbrandt, 2001). The basin is separated structurally by the Zelten Platform into western and eastern sub-basins (Hallett, 2002), the former, in particular the Zallah Trough (Fig. 1B, C) in onshore north-central Libya (Concession 11), being the focus of this paper.

The North African region was subjected to diachronous rifting and subsequent post-Mesozoic continental collision, which led to the development in Libya of basins with complex origins. A number of different tectonic domains existed, each having a unique history (Carr, 2003).

The Sirte Basin region is a major intracratonic rift system on the north-central African plate. The structural developments of this region through geological time have been discussed previously (Massa and Delort, 1984). It was a positive feature until the latest Jurassic when the area gradually subsided, probably for the first time since the Early Palaeozoic. Subsidence resulted from extension that led to the collapse of the pre-existing Sirte Arch (Anketell, 1996). The area experienced stretching and down-faulting during the Cretaceous Period. Large scale subsidence and block faulting began in the latest Jurassic/Early Cretaceous (Abadi et al., 2008), creating a complex of horsts and grabens. The faults in the Sirte Basin were reactivated during the Late Cretaceous, movement involving thermal arching and repeated phases of rifting, especially during this period and in the Paleocene–Eocene, when subsidence of the basin reached a maximum (Gumati and Kanes, 1985; Abadi et al., 2008). Volcanic activity resumed in post-Eocene times. This is believed to have been concurrent with movement along major basement fault zones situated outside the Cretaceous rift on the western side of the basin.

The sedimentary succession of the Sirte Basin naturally reflects its tectonic and structural evolution, which was closely related to the opening of the Atlantic Ocean and convergence of the Tethys region during the Mesozoic and Cenozoic eras (Gras and Thusu, 1998). According to El-Alami (1996), the history of the basin during the Late Cretaceous consisted of a gradual on-lap of the fault-block topography by marine sediments so that by the very end of the period almost all of the topographic highs were buried.

4. Material and methods

This paper focuses on 14 wells located in Concession 11, western Sirte Basin (Fig. 1A; Table 1). One hundred and thirty-six samples (94 cores and 42 ditch cuttings; Tables 2, 3) were available for study. These and basic data were kindly provided by Harouge Oil Operations (previously Veba Oil Operations), Tripoli, Libya. The data for these wells straddle Upper Cretaceous–Eocene deposits in several oil fields, namely the Tagrifet, Daba, Ghani/Farrud, Abeter, Mellugh, and Ed Dib (Fig.1A).

4.1 Organic geochemical analyses

Fifty-six Upper Cretaceous samples (14 cores and 42 cuttings) from 14 exploration wells (QQQ1, LLL1, RRR45, RRR32, RRR29, RRR40, RRR28, RRR25, RRR76, AA1, RRR1, FFF1, GG1, and HHH1) were analyzed (Fig. 1C; Table 1). Not all Rock-Eval analyses were carried out on the same samples selected for palynofacies, petrographic and microfacies studies, those chosen being regarded as representative of the prime source rocks in the succession studied. Each sample was combusted in an oxidation oven to obtain the weight percent of residual carbon and oxidized mineral carbon. The oven temperature programme for pyrolysis was 300°C isothermal for 3 min followed by a 25°C/min ramping from 300°C to 650°C. The oxidation programme was 300°C isothermal for 30 s followed by a 25°C/min increasing from 300°C to 850°C, held isothermal for 5 min at 850°C. The released hydrocarbons were continuously detected with a flame ionization detector (FID), whereas CO and CO_2 released during pyrolysis and oxidation of the samples were measured using online infrared cells (IR). This was done to determine total organic carbon (TOC), hydrogen index (HI), T_{max} and other parameters to screen the kerogen type, depositional environment, maturity of the organic matter and petroleum generative potential of the samples. All of these analyses were carried out at the StratoChem Laboratory, New Maadi, Cairo, and GeoMark Research Limited, Houston, Texas.

4.2 Palynofacies analysis

Eighty cuttings and core samples from the Upper Cretaceous Bahi, Etel, Rachmat, Sirte and Kalash formations, the Paleocene Zelten Formation and Farrud Member of the Beda Formation, and the Paleocene–Eocene Kheir Formation encountered in seven wells (QQQ1, LLL1, RRR40, AA1, FFF1, GG1 and HHH1: Fig. 1C, Table 3) were processed for palynofacies analysis in the Petroleum and

Paleontology Laboratory, Department of Geology, Mansoura University using standard extraction techniques (El Beialy et al., 2016). The selection of the samples investigated for palynofacies analysis was based mostly on lithologies ranging from shales and mudstones to limestones, which yielded different types and amounts of organic matter, but few palynomorphs overall. Nearly 10 g of each sample were crushed in a Pyrex mortar; carbonates were then removed by immersion in 35% HCl in a glass beaker until effervescence ceased. This was followed by repeated dilution with distilled water and decanting until the samples were neutral. The residues were transferred to plastic pots to which 40% HF was added for 3–7 days and stirred once a day. During this period, some HF was decanted also once a day and fresh acid added. The samples were then washed with distilled water, decanting daily until they were neutral. Unwanted particles were separated from these using 125 μm mesh brass and 10 μm mesh nylon sieves to remove coarse and very fine particles respectively. A small amount of each residue was pipetted off, evenly spread on a glass coverslip and left to dry at about 20^{o}C, followed by mounting on a glass slide using Elvacite 2044 as a mounting medium. Excess Elvacite was removed by soap and water to make the slide clean and ready for examination. Transmitted light microscopy was used to scan the slides for their kerogen content. Two slides were prepared from each sample and, whenever possible, about 200 particles were point counted in order to calculate relative abundances and represent quantitatively the different kerogen categories: most of the samples were poorly fossiliferous. The amounts recorded were categorized as abundant (>35%), frequent (16–35%), common (5–15%) or rare (<5%) (Table 3). All slides were examined fully under a 40× objective to check for the presence of any rare palynomorphs. Observations were made under an Olympus BX51 (E330-ADU1.2X) transmitted light microscope and photomicrographs taken with an Olympus digital camera. All microscope slides and residues are housed in the Department of Geology, Mansoura University.

4.3 Petrographic and microfacies examination

The samples selected for analysis were mainly limestones and dolomites: by contrast with the palynofacies analysis no clastic deposits were investigated. In the succession studied, major reservoirs occur in the Upper Cretaceous–Eocene non-clastic sediments, mainly in the Farrud and Mabruk members of the Zelten Formation.

Thin sections of 80 rock samples were prepared using a rock saw and then ground flat before being impregnated with epoxy resin, mounted on glass slides, and ground and polished using carbide grit until they were about 0.03 mm thick before being covered by glass cover slips. An Olympus BX51

polarizing microscope was used for petrographic analysis and photomicrographs were taken digitally, the aim being to determine facies distributions as well as the mineral and fossil content.

5. Results and discussion

5.1. TOC and Rock-Eval pyrolysis

Use of core and hand-picked cuttings samples made it easy to overcome contamination problems resulting from drilling mud additives and caving from younger horizons when analyzing TOC content and kerogen typing. This is apparent in the plot of Rock-Eval S_1 (mg HC/g rock) versus TOC (Fig. 3) in which all the hydrocarbons released are indigenous (in situ) and there is no possibility of contamination (Mukhopadhyay et al., 1995; Hunt, 1996).

The TOC content of the samples varies between 0.19 and 2.04 wt%. Nearly half have TOC contents of <1.0 wt%. These low values may be a result of dilution, which does not reduce the amount of organic matter preserved, but does spread it more thinly through the rock. The samples analyzed are mostly shales, but include some carbonates. The shales are strongly diluted, and facies changes from carbonates to shales may also be associated with large dilution effects (Waples, 1985; Bohacs et al., 2000). An appropriate combination of maximum production of organic matter and minimal destruction and dilution will enhance organic enrichment and lead to the formation of potential source rocks (Bohacs et al., 2000). Although the TOC content of many of the samples examined is low, at least it is >1.0 wt% in the majority, and in one sample from the Kalash Formation in well FFF1.9 at depth 2380 m (Table 2) m it is 2.04 wt% and has elevated S_2 values (6.96 mg HC/g rock).

The Rock-Eval S_2 values are <2.0 mg HC/g rock for almost all Etel and Rachmat samples (Table 2; Fig. 4). In addition, the low hydrogen indices of <150 mg HC/g TOC for these formations indicate the absence of significant amounts of oil generative lipid materials and kerogen that is mainly Type III or Type IV (Fig. 5). It is highly unusual to encounter a rock in which the TOC is approximately 0.5% and the hydrogen index is nearly 400, because the extensive oxidation indicated by low TOC values almost always results in the loss of hydrogen-rich material (Waples, 1985; El Diasty et al., 2016a). On the other hand, the high hydrogen indices of >150 mg HC/g TOC and oxygen-depleted terrigenous organic matter (Table 2; between 150 and 300 mg HC/g TOC) for the samples from the Sirte and Kalash formations reflect Type II/III kerogen (Fig. 5) and therefore indicate marginal to fair potential for liquid hydrocarbons (Waples, 1985; Peters and Cassa, 1994). The increasing proportions

of lipid-rich material, either from terrestrial or marine algal organic matter, for the samples from the Sirte Formation may indicate a higher proportion of oil-generative kerogen compared to the other rock units (El Diasty et al., 2016b).

The T_{max} values for the Upper Cretaceous section in the western Sirte Basin vary with kerogen type and the mineralogy of the rock as well as maturity. Our data suggest that most of the samples lie within the early mature zone (Fig. 6) of hydrocarbon generation (430–447°C; Espitalié et al., 1985). Two samples from the Etel Formation in the AA1 well (AA1.10 and AA1.12) have T_{max} values of 425 and 424°C respectively (Table 2), which indicate that they are immature (Fig. 6).

5.2 Palynofacies and sedimentary facies

There are few palynofacies-orientated publications on Libyan Phanerozoic deposits. Thusu et al. (1988) and Uwins and Batten (1988) evaluated Jurassic to mid Cretaceous strata and facies in north-east Libya, and more recently Paris et al. (2012) reported on the palynology and palynofacies of the Early Silurian Tanezzuft Formation in the eastern Murzuq Basin. There is a single report on the palynology and palynofacies of Upper Cretaceous deposits in well C275-65 in the Sirte Basin (Bu-Argoub, 1996) and, on a related matter, a description of a new dinocyst species (*Odontochitina tabulata*) from a late Santonian–early Campanian deposit in well C3-65 in the basin (El-Mehdawi, 1998).

The results of our palynofacies analysis of samples from the Concession 11 wells are discussed below in chronological order beginning with the oldest formation:

Bahi Formation: wells LLL1 and AA1, four and three samples respectively: all are dominated by terrigenous amorphous organic matter (AOMT) and phytoclasts. The AOMT has a gelified appearance with no internal structure (Batten, 1983; Ercegovac and Kostić, 2006). The percentage of phytoclasts is between 68 and 71% in well AA1, and 56 and 73% in well LLL1. The absence of dinocysts and microforaminiferal test linings indicates a lack of marine influence, as has been indicated previously for the lower part of the formation. This confirms Hallett's (2002) observation that the palynomorph content of the Bahi Formation in the As Sarir Field suggests a non-marine depositional setting. The upper part of the formation contains rare palynomorphs assigned to the dinocyst *Senegalinium granulostriatum* Jain & Millepied (Fig. 7A) associated with glauconite, which could be part of the overlying marine cycle (Barr and Weegar, 1972).

Etel Formation: 19 samples, wells QQQ1 (6 samples), LLL1 (5), AA1 (5), FFF1 (2) and GG1 (1): all contain mainly phytoclasts and AOMT. The percentage of phytoclasts in the QQQ1, LLL1, AA1, and GG1 samples is usually more than 50% of the total particulate organic matter. They consist mainly of pale brown to brown, well- to fairly well-preserved structured terrestrial plant fragments: mostly tracheids, cuticles and woody tissues (Fig. 7B, C). *Pediastrum* is the most common palynomorph taxon in the LLL1 well, especially at 2853–2855 m (Fig. 7D). The stratigraphic range of this colonial chlorococcalean green alga extends back to the Lower Cretaceous (Evitt, 1963). It is generally a good freshwater indicator (Batten 1996; Mendonça Filho et al., 2010), and most abundant in freshwater to low salinity tropical and subtropical lakes (Tyson, 1995). When abundant it may also indicate important source rocks in Cretaceous and Cenozoic rift basins (Hutton, 1988; Batten, 1996). In marine sediments, it can be used as an indicator of relative proximity to fluvio-deltaic source areas or reflect transport from these areas (Tyson, 1993, 1995; Batten, 1996; Mendonça Filho et al., 2010). The ternary plot (Fig. 8) indicates that the Etel samples fall mainly within the II (kerogen Type III) and VI (kerogen Type II) fields.

Rachmat Formation: wells GG1 and HHH1, four and two samples respectively: all are again dominated by phytoclasts and AOMT. The phytoclast component comprises between 65 and 85% of the particulate organic matter, with palynomorphs not amounting to more than 2%, the rest of the organic matter being AOMT. All fall within field II (kerogen Type III) of the ternary plot, reflecting deposition in a marginal dysoxic–anoxic basin (Fig. 8). Anoxic marine shales in the As Sarir Field on the south-east margin of the Sirte Basin that contain Turonian–early Campanian palynomorphs are probably equivalent to the Rachmat Formation (Hallett, 2002).

Sirte Formation: 27 samples, wells QQQ1 (1 sample), RRR40 (7), AA1-11 (3), FFF1 (1), GG1 (9) and HHH1 (6). Phytoclast percentages in these samples range from 12–75%, but AOM is the dominant component of the majority. This is mostly bacterially degraded algal matter (AOMA; Batten, 1996), AOMT (Fig. 7E) being generally subordinate. Palynomorphs never amount to more than 5% of the assemblage (Fig. 7F). The phytoclasts consist mainly of cuticles and wood fragments, including tracheids, which are sometimes biodegraded. Their angular shapes reflect limited transportation. The ternary diagram (Fig. 8) places the samples within fields II (marginal dysoxic–anoxic basin), IX (distal suboxic–anoxic basin) and (one only) IV (shelf to basin transition). Kerogen types are III and II>I. This

is in accordance with the findings of Hallett (2002) who documented nearly 75 m of anoxic, marginal marine shales containing abundant Campanian marine palynomorphs from the same formation in the As Sarir Field.

Microfacies analysis of the four core samples available from the AA1 and FFF1 wells indicates deposition of laminated sandy mud biomicrite (Fig. 9A) changing upward to pelagic foraminiferal mud micrite (Fig. 9B), signifying deposition initially in relatively shallow, moderate energy conditions within an inner to mid shelf above base level, followed by deeper environments as sea level continued to rise.

Kalash Formation: AA1 and FFF1 wells, four and ten samples respectively. AOM amounts to no less than 49% in all of the samples, phytoclasts making up the bulk of the rest of the particulate organic matter counted, with palynomorphs amounting to no more than 7% (Fig. 7G, H). Although generally rare, some of the palynomorphs are biostratigraphically diagnostic (e.g., *Palaeocystodinium australinium*; Fig. 7F) and ecologically significant (e.g., *Tasmanites*; Fig. 7G). *Palaeocystodinium australinium* is typical of Maastrichtian and Paleocene strata (e.g., Schrank, 1984 and citations therein). May (1980) reported a *Palaeocystodinium* peak zone in New Jersey (USA) that was dated as Maastrichtian. This dinoflagellate inhabited normal marine waters of a near-shore gulf environment during the deposition of the Kalash Formation, which took place during a marine regression. This is closely comparable to palaeoenvironmental conditions reported for a *Palaeocystodinium* association in Egypt (Schrank, 1984). The ternary plot shows that most samples fall within field IX (kerogen Type II>I), reflecting a distal suboxic–anoxic basin, but some are in field II (kerogen Type III) indicating similar conditions but in a shelf environment (Fig. 8). This supports the conclusion of Barr and Weegar (1972) that the Kalash Formation was deposited in open marine, probable neritic conditions during the Maastrichtian.

Our microfacies analysis also indicates that deposition of this formation took place during the Maastrichtian on an outer shelf when sea levels were high. The microfacies associations of five core samples from the AA1 and FFF1wells are dominated by a pelagic foraminiferal biomicrite association/foraminiferal packstone (Fig. 9C). This is mainly composed of a microcrystalline micritic matrix with a laminated structure, grain-supported sand-sized allochems dominated by pelagic foraminiferal chambers (rounded globigerinids), *Nummulites*, miliolids, bivalve fragments, gastropods and black framboidal pyrites.

Farrud Member of the Beda Formation: GG1 well, three samples, all dominated by aquatic amorphous organic matter (AOMA); phytoclasts comprise a maximum of 48% and palynomorphs 5%. The AOMA has a fluffy or flakey granular texture, suggesting derivation from autotrophic or heterotrophic phytoplankton or bacteria (Tyson, 1995; Ercegovac and Kostić, 2006; Mendonça Filho et al., 2010), which is equivalent to the bacterially degraded algal matter of Batten (1996). According to Barr and Weegar (1972), the Farrud Member is composed of 45 m of intertidal dolomites that accumulated in shallow water with moderate wave and current activity in tropical conditions. This is supported palynologically by the presence of microforaminiferal test linings in the samples examined. All three samples are located in field VI (kerogen Type II, Fig. 8), indicating a proximal suboxic–anoxic shelf (Tyson, 1993).

Microfacies data from 46 core samples indicate that the deposition of the Farrud Member began in shallow supratidal and intertidal settings, dolostone and evaporite facies having been identified in the samples from the QQQ1, LLL1 and RRR45 wells (Fig. 9D). By contrast, those from wells GG1, RRR1 and RRR40 indicate deposition in an inner-shelf environment at a time of maximum sea-level rise. During this period, laminated, ferruginous sandy muds were deposited mainly in relatively quiet, low-energy, inner shelf–lagoonal marine settings (Fig. 9E).

Zelten Formation: Only two representative samples from the HHH1 well have been examined. Both contain a lot of AOMA (48–52 %) along with phytoclasts (45–50%) and very much subordinate palynomorphs (2–3%) (Fig. 7I–L), most of which are dinocysts referable to *Chatangiella* sp. and *Dinogymnium* sp. These are widely regarded as Upper Cretaceous markers, although records of both genera are known from Paleocene and even Eocene strata (Traverse, 2007). The alleged Tertiary occurrences are rare and sporadic, and the possibility of reworking cannot be excluded. Both samples are within field VI (kerogen Type II) of the ternary plot, suggesting deposition on a proximal suboxic–anoxic shelf (Fig. 8). This is supported by the occurrence of the *Chatangiella*, because it is an indicator of relatively near-shore, inner-shelf environments (Thorn et al., 2009; Arai and Viviers 2013) in which terrigenous input was significant. The *Dinogymnium* occurrences probably indicate similar conditions (Schrank, 1984).

Kheir Formation: well AA1, two samples, one of which (from 1728 m) is dominated by AOMA (85%) and includes resin: the remainder of the palynofacies comprises 14% phytoclasts and 1% palynomorphs including microforaminiferal test linings (Fig. 7M–P), which supports deposition in a

shallow marine setting (Stancliffe, 1989). The other sample (from 1902 m) is also dominated by AOMA (79%; Fig. 7P), the remainder mostly comprising phytoclasts (20%: wood and cuticles), with again only a very small number of palynomorphs in association. The AOM contains an abundance of pyrite crystals, resulting from the activity of sulfur-reducing bacteria in stagnant (oxygen-depleted) water at the site of deposition (Batten, 1983; Ercegovac and Kostić, 2006). This sample falls within field IX (Fig. 8) indicating a distal basin and Type II>I kerogen, reflecting a restricted, oxygen-deficient marine setting.

The microfacies associations in 13 core samples from this formation indicate that deposition took place during a period of oscillating sea level in relatively low to high energy, shallow marine, middle to outer shelf conditions interspersed with short-lived, shallow intertidal–lagoonal to supratidal episodes. Toward the top of the formation there are indications of deposition during a marked lowering of sea level in the form of dolomite and evaporitic dismicrite (Fig. 9F) that accumulated in warm, shallow, intertidal and supratidal conditions. This is again supported palynologically by the presence of microforaminiferal test linings.

5.3 Palynofacies associations

Two palynofacies associations linked to kerogen type and depositional environments have been identified as follows:

Palynofacies association-A (PF-A): samples of Association-A lie mainly within field II in the ternary APP plot (Fig. 8). This indicates a marginal dysoxic–anoxic basin and Type III, gas-prone kerogen (Tyson, 1995). The association was recorded from 39 samples from four formations: Bahi (6), Etel (15), Rachmat (6) and Sirte (12).

Palynofacies association-B (PF-B): Association-B samples lie within palynofacies fields VI and IX in the ternary plot, showing a clear transition from a proximal suboxic–anoxic shelf and Type II kerogen to an oil-prone, distal suboxic–anoxic basin. Forty-one samples are referable to this association. These are from the Bahi (1), Etel (4), Sirte (15), Kalash (14), Beda (Farrud Member) (3), Zelten (2) and Kheir (2) formations.

Facies distributions are difficult to correlate between wells, which suggests that there was a strong tectonic control on sediment deposition, including differential subsidence. Differing stratigraphic positions and numbers of transgressive–regressive cycles in each well make formation-wide correlation problematic (Swei, 2010). In order to portray the depositional regime in the study area

of Concession 11, we have constructed a conceptual model for the sedimentary environment of the Upper Cretaceous succession (Fig. 10A). This shows that the sediments concerned were initially deposited in relatively shallow, moderate energy conditions within an inner to mid shelf above base level, followed by deeper environments as sea level rose. A similar reconstruction for the overlying Paleocene–Eocene succession (Fig. 10B) shows relatively shallow marine sedimentation in mid to outer shelf environments alternating with short-lived, shallow, intertidal-lagoonal to supratidal conditions.

5.4 Integration of palynofacies and organic geochemical results

Integration of palynofacies and geochemical data is more effective for assessing the hydrocarbon potential of source rocks than relying on one or other method on its own (e.g., El Diasty et al., 2014). Our combined data from four formations (Etel, Rachmat, Sirte, and Kalash) in seven wells (QQQ1, LLL1, RRR40, AA1, FFF1, GG1 and HHH1) are plotted on Table 4 and enable the recognition of two possible oil/gas and gas source rock horizons, as follows:

Immature to early mature gas-prone source rocks are suggested to be within the Etel, Rachmat and Sirte formations in the QQQ1, LLL1, AA1, FFF1 and GG1 wells. This is based on the dominance of AOM (which is mostly terrestrially derived) with abundant phytoclasts and opaque detritus in association. The TOC of the Etel Formation is 0.35–0.88 wt% with pyrolysis S_2 yields of 0.31–0.84 mg HC/g rock and an HI of 71.18–163.96 mg HC/g TOC. The TOC of the Rachmat Formation is 0.77–1.22%, pyrolysis S_2 yields are 0.83–1.4 mg HC/g rock and the HI is 92.71–129.53 mg HC/g TOC. These results indicate biogenic gas to onset oil generation for this part of the succession.

Mature oil/gas-prone source rocks are considered to occur in the Sirte and Kalash formations penetrated by the FFF1, HHH1, RRR40, QQQ1 and GG1 wells (Table 4). These formations contain deposits that range from yielding an average amount of organic matter to being very organic-rich (TOC 0.57–1.72 wt % for the Sirte and 0.58–2.04 wt% for the Kalash formations respectively). They have fair potential to generate oil/gas: pyrolysis S_2 yields of 0.47–3.73 mg HC/g rock and an HI up to 288.69 for the Sirte Formation, and pyrolysis S_2 yields of 1.11–6.96 mg HC/g rock and an HI of 190.72–341.17 mg HC/g TOC for Kalash Formation, both with palynomorphs that indicate thermal maturity. Peak oil generation is suggested for these formations.

6. Conclusions

The Upper Cretaceous–Eocene succession in the study area begins with the Bahi Formation, the lower part of which is comparable to the pre-Upper Cretaceous Nubian facies in having been deposited mainly under a non-marine regressive phase, as indicated by the absence of dinocysts and microforaminiferal test linings. By contrast, the upper part reflects a marine setting.

Data on the Turonian Etel Formation indicate an anoxic sabkha/lagoonal environment at a time of high relative sea level. The Coniacian–Santonian Rachmat Formation contains foraminifera and ostracodes that imply a marine environment. Palynological evidence suggests deposition under marginal marine, dysoxic–anoxic conditions.

The palynological and microfacies data obtained from the Campanian Sirte Formation indicate deposition in a relatively shallow, fairly high energy marine environment within inner to mid shelf embayments above base level, but with continuous sea-level rise leading to deeper environments in a marginal dysoxic–anoxic basin, and suboxic–anoxic shelf conditions. Microfacies analysis indicates that the Maastrichtian Kalash Formation accumulated in a marine shelf environment at a time of high sea level. Palynological data confirm deposition under proximal–distal suboxic–anoxic conditions, as evidenced by the presence of the dinocysts *Palaeocystodinium* and *Dinogymnium*, both being indicators of relatively near-shore, inner-shelf marine environments.

The lower Paleocene, Selandian, Farrud Member of the Beda Formation reflects deposition in shallow supratidal and intertidal sub-environments alternating with deeper water conditions of shelf embayments at a time of maximum sea-level rise. This interpretation is supported palynologically by the presence of shallow marine microforaminiferal test linings in the palynofacies. The Paleocene, Thanetian, Zelten Formation was deposited in a relatively deep marine environment despite being associated with a remarkable lowering of sea level. Palynological evidence indicates sedimentation in a proximal suboxic–anoxic shelf environment that favoured the preservation of the dinocysts *Chatangiella* and *Dinogymnium*. Facies of the uppermost Thanetian–Ypresian Kheir Formation were deposited under oscillating sea levels, relatively shallow mid- to outer-shelf conditions alternating with those reflecting short-lived, shallow, intertidal–lagoonal to supratidal situations, the continuing regression being indicated by the accumulation of dolomite and evaporitic dismicrite in shallow marine environments.

Two palynofacies associations linked to kerogen type and depositional conditions have been recognized. Association-A samples lie mainly within field II in the APP ternary plot, indicating a

marginal dysoxic–anoxic basin and Type III, gas-prone kerogen. Association-B samples fall within palynofacies fields VI and IX showing a clear transition from a proximal suboxic–anoxic shelf and Type II kerogen to an oil-prone, distal suboxic–anoxic basin.

The integration of the visual kerogen and organic thermal maturity data led to the recognition of two possible oil/gas and gas source-rock horizons in the wells studied. Based on the dominance of AOM (which is mostly terrestrially derived) and abundant phytoclasts and opaque detritus, immature to early mature gas-prone source rocks are suggested to occur in the Etel and Rachmat formations leading to biogenic gas and onset oil generation. Mature oil/gas-prone source rocks are suggested to be within the Sirte and Kalash formations. These formations contain average to large amounts of organic matter and palynomorphs that indicate organic maturity, implying fair potential to generate oil/gas and peak oil generation.

Acknowledgements

We are indebted to Harouge Oil Operations for the provision of samples, geological information and permission to publish this study, and to StratoChem, New Maadi, Cairo and GeoMark, Houston, Texas for laboratory assistance and running all of the analyses for geochemical investigation. We sincerely thank Editor-in-Chief, Vural Suicmez, and two anonymous reviewers for constructive comments on an earlier version of this manuscript.

References

Abadi, A.M., van Wees, J.-D., van Dijk, P.M., Cloetingh, S.A.P.L., 2008. Tectonics and subsidence evolution of the Sirt Basin, Libya. AAPG Bulletin 92, 993–1027.

Ahlbrandt, T.S., 2001. The Sirte Basin province of Libya–Sirte-Zelten total petroleum system. US Geological Survey Bulletin 2202-F, http://geology.cr.usgs.gov/pub/bulletins/b2202-f, pp. 1–29.

Anketell, J.M., 1996. Structural history of the Sirt Basin and its relationship to the Sabrata and Cyrenaica Platform, northern Libya. In: Salem, M.J., El-Hawat, A.S., Sbeta, A.M. (Eds.), The Geology of the Sirt Basin, 3. Elsevier, Amsterdam, pp. 57–88.

Arai, M., Viviers, M.C., 2013. Dinoflagellate cyst super dominance assemblages from the Upper Cretaceous of the Santos Basin, offshore SE Brazil, and their palaeoecological significance. In: Lewis, J.M., Marret, F., Bradley, L. (Eds.), Biological and geological perspectives of

dinoflagellates. The Micropalaeontological Society, Special Publications. Geological Society of London, pp. 285–292.

Barr, F.T., Weegar, A.A., 1972. Stratigraphic nomenclature of the Sirt Basin, Libya. The Petroleum Exploration Society of Libya, Tripoli, Libya, 179 pp.

Batten, D.J., 1983. Identification of amorphous sedimentary organic matter by transmitted light. In: Brooks, J. (Ed.), Petroleum Geochemistry and Exploration of Europe. Geological Society, London, Special Publication 12, 275–287.

Batten, D.J., 1996. Palynofacies and palaeoenvironmental interpretation. In: Jansonius, J., McGregor, D.C. (Eds.), Palynology: Principals and Applications. Vol. 3. American Association of Stratigraphic Palynologists' Foundation, Dallas, pp. 1011–1064.

Bohacs, K.M., Carroll, A.R., Neal, J.E., Mankiewicz, P.J., 2000. Lake-basin type, source potential, and hydrocarbon character: an integrated-sequence-stratigraphic–geochemical framework. In: Gierlowski-Kordesch, E.H., Kelts, K.R. (Eds.), Lake Basins through Space and Time. AAPG Studies in Geology 46, pp. 3–34.

Bu-Argoub, F.M., 1996. Palynological and palynofacies studies of the Upper Cretaceous sequence in well C275-65, Sirte Basin, NE Libya. In: Salem, M.J., Mouzughi, A.J., Hammuda, O.S. (Eds.), The Geology of the Sirte Basin, 1. Elsevier, Amsterdam, pp. 418–453.

Carr, I.D., 2003. A sequence stratigraphic synthesis of the North African Mesozoic. Journal of Petroleum Geology 26, 133–152.

El-Alami, M., 1996. Habitat of oil Abu Attifel area Sirt Basin, Libya. In: Salem, M.J., Busrewil, M.T., Misallati, A.A., Sola, M.A. (Eds.), The Geology of the Sirt Basin, 2. Elsevier, Amsterdam, pp. 337–347.

El Beialy, S.Y., Zobaa, M.K., Taha, A.A., 2016. Depositional paleoenvironment and hydrocarbon source potential of the Oligocene Dabaa Formation, north Western Desert, Egypt: a palynofacies approach. Geosphere 12, 346–353.

El Diasty, W.Sh., El Beialy, S.Y., Abo Ghonaim, A.A., Mostafa, A.R., El Afty, H., 2014. Palynology, palynofacies and petroleum potential of Upper Cretaceous–Eocene Matulla, Brown Limestone and Thebes formations, Belayim oilfields, central Gulf of Suez, Egypt. Journal of African Earth Sciences 95, 155–167.

El Diasty, W.Sh., El Beialy, S.Y., Littke, R., Farag, F.A., 2016a. Source rock evaluation and nature of hydrocarbons in the Khalda Concession, Shushan Basin, Egypt's Western Desert. International Journal of Coal Geology 162, 45–60.

El Diasty, W.Sh., El Beialy, S.Y., Peters, K.E., El Atfy, H., Gheith, A.M., Agha, N.N., 2016b. Organic geochemistry of crude oils and Upper Cretaceous source rocks from Concession 11, west Sirte Basin, Libya. Journal of Petroleum Geology 39, 393–413.

El-Mehdawi, A.D., 1998. *Odontochitina tabulata* sp. nov. A late Santonian–early Campanian dinoflagellate cyst from SE Sirte Basin, Libya. Journal of Micropalaeontology 17, 173–178.

Ercegovac, M., Kostić, A., 2006. Organic facies and palynofacies: nomenclature, classification and applicability for petroleum source rock evaluation. International Journal of Coal Geology 68, 70–78.

Espitalié, J., Deroo, G., Marquis, F., 1985. Rock Eval pyrolysis and its applications. Revue de l'Institut Français du Pétrole 40, 563–579.

Evitt, W.R., 1963. Occurrence of freshwater alga *Pediastrum* in Cretaceous marine sediments. American Journal of Science 261, 890–893.

Gras, R., Thusu, B., 1998. Trap architecture of the Early Cretaceous Sarir Sandstone in the eastern Sirt Basin, Libya. In: MacGregor, S.D., Moody, J.T.R., Clark-Lowes, D.D. (Eds.), Petroleum Geology of North Africa. Geological Society, London, Special Publication 132, pp. 317–334.

Gumati, Y.D., Kanes, W.H., 1985. Early Tertiary subsidence and sedimentary facies, north Sirt Basin, Libya. AAPG Bulletin 69, 39–52.

Hallett, D., 2002. Petroleum geology of Libya. Elsevier, Amsterdam, 502 pp.

Hunt, J., 1996. Petroleum geochemistry and geology. W.H. Freeman, New York, 743 pp.

Hutton, A.C., 1988. The lacustrine Condor oil shale sequence. In: Fleet, A.J., Kelts, K., Talbot, M.R. (Eds.), Lacustrine Petroleum Source Rocks. Geological Society, London, Special Publication 40, pp. 329–340.

Jain, K.P., Millepied, P., 1973. Cretaceous microplankton from Senegal Basin, NW Africa. 1. Some new genera, species and combinations of dinoflagellates. The Palaeobotanist 20, 22–32.

Lentin, J.K., Williams, G.L., 1976. A monograph of fossil peridinioid dinoflagellate cysts. Bedford Institute of Oceanography, Report Series, no.BI-R-75-16, 237 p.

Massa, D., Delort, T., 1984. Evolution du Bassin de Syrte (Libye) du Cambrien au Crétacé basal. Bulletin de la Société Géologique de France, Série 7, 26, 1087–1096.

May, F.E., 1980. Dinoflagellate cysts of the Gymnodiniaceae, Peridiniaceae, and Gonyaulacaceae from the Upper Cretaceous Monmouth Group, Atlantic Highlands, New Jersey. Palaeontographica, Abteilung B 172, 10–116.

Mendonça Filho, J.G., Chagas, R.B.A., Menezes, T.R., Mendonça, J.O., da Silva, F.S., Sabadini-Santos, E., 2010. Organic facies of the Oligocene lacustrine system in the Cenozoic Taubaté Basin, southern Brazil. International Journal of Coal Geology 84, 166–178.

Mukhopadhyay, P.K., Wade, J.A., Kruge, M.A., 1995. Organic facies and maturation of Jurassic/Cretaceous rocks, and possible oil-source rock correlation based on pyrolysis of asphaltenes, Scotian Basin, Canada. Organic Geochemistry 22, 85–104.

Paris, F., Thusu, B., Rasul, S., Meinhold, G., Strogen, D., Howard, J.P., Abutarruma, Y., Elgadry, M., Whitham, A.G., 2012. Palynological and palynofacies analysis of early Silurian shales from borehole CDEG-2a in Dor el Gussa, eastern Murzuq Basin, Libya. Review of Palaeobotany and Palynology 174, 1–26.

Peters, K.E., Cassa, M.R., 1994. Applied source rock geochemistry. In: Magoon, L.B., Dow, W.G. (Eds.), The Petroleum System–from Source to Trap. AAPG Memoir, 60, pp. 93–120.

Schrank, E., 1984. Organic-geochemical and palynological studies of a Dakhla Shale profile (Late Cretaceous) in southeast Egypt. Part A: Succession of microfloras and depositional environments. Berliner Geowissenschaftliche Abhandlungen A 50, 189–207.

Stancliffe, R.P.W., 1989. Microforaminiferal linings: their classification, biostratigraphy and paleoecology, with special reference to specimens from British Oxfordian sediments. Micropaleontology 35, 337–352.

Swei, G.H., 2010. Sedimentology, diagenesis and reservoir characteristics of Eocene carbonates, Sirt Basin, Libya. Unpublished PhD thesis, Durham University, UK, 220 p.

Thorn, V.C., Riding, J.B., Francis, J.E., 2009. The Late Cretaceous dinoflagellate cyst *Manumiella* – biostratigraphy, systematics, and palaeoecological signals in Antarctica. Review of Palaeobotany and Palynology 156, 436–448.

Thusu, B., Van der Eem, J.G.L.A., El-Mehdawi, A.D., Bu-Argoub, F., 1988. Jurassic–Early Cretaceous palynostratigraphy in northeast Libya. In: El-Arnauti, A., Owens, B., Thusu, B. (Eds.), Subsurface Palynostratigraphy of Northeast Libya. Garyounis University Publications, Benghazi, Libya (SPLAJ), pp. 171–213.

Traverse, A., 2007. Paleopalynology, 2nd edition. Springer, Dordrecht, 813 pp.

Tyson, R.V., 1993. Palynofacies analysis. In: Jenkins, D.G. (Ed.), Applied Micropaleontology. Kluwer, Dordrecht, pp. 153–191.

Tyson, R.V., 1995. Sedimentary organic matter. Chapman and Hall, London, 615 pp.

Uwins, P.J.R., Batten, D.J., 1988. Early to mid-Cretaceous palynology of northeast Libya. In El-Arnauti, A., Owens, B., Thusu, B. (Eds.), Subsurface Palynostratigraphy of Northeast Libya. Garyounis University Publications, Benghazi, Libya (SPLAJ), pp. 215–257.

Waples, D.W., 1985. Geochemistry in Petroleum Exploration. D. Reidel, Dordrecht, 232 pp.

Figure and table captions

Fig. 1. A, Location map of the study area in Concession 11, western Sirte Basin, northern Libya, modified from El Diasty et al. (2016b) after Ahlbrandt (2001); **B**, the main structural elements in the Sirte Basin; **C**, spatial distribution of kerogen particles recorded from the wells studied.

Fig. 2. Lithostratigraphic column for the Concession 11 area: modified by El Diasty et al. (2016b) after Barr and Weegar (1972).

Fig. 3. Plot of S_1 versus TOC, on which migrated or contaminating hydrocarbons can be distinguished from indigenous hydrocarbons.

Fig. 4. Plot of TOC versus S_2 for the Upper Cretaceous source rock samples from Concession 11.

Fig. 5. Data on hydrogen and oxygen indices plotted on a pseudo-van Krevelen diagram (from Espitalié et al., 1985) for the Upper Cretaceous source rock samples from Concession 11.

Fig. 6. Plot of hydrogen index (HI) versus T_{max} for source rock samples from Concession 11.

Fig. 7. Bright field transmitted light photomicrographs of selected kerogen particles and palynomorphs from rock units in the wells investigated. Well name and sample number combined (e.g., HHH1.3) and corresponding depth (e.g., 2351–2353 m) follow the identification of each specimen. Sizes indicated by scale bars on the images. A, *Senegalinium granulostriatum* Jain & Millepied 1973, Bahi Formation; LLL1.8, LLL1, 3032–3036 m. B, Woody matter showing rectangular cell structure, Etel Formation; GG1.17, 3051 m. C, Cuticle, Etel Formation; LLL1.3, 2853–2855 m. D, *Pediastrum*, Etel Formation; LLL1.3, LLL1 well, 2853–2855 m. E, AOMT containing much pyrite (arrows), Sirte Formation; HHH1.4, 2362–2365 m. F, *Palaeocystodinium australinium* (Cookson) Lentin & Williams 1976, Kalash Formation; FFF1.9, FFF1 well, 2380 m. G, *Tasmanites* sp., Kalash Formation; FFF1.1, FFF1 well, 2372 m. H, AOMT with relict cellular structure (arrows), Kalash Formation; FFF1.10, FFF1 well, 2382 m. I, *Dinogymnium* sp., Zelten Formation; HHH1.2, HHH1 well, 1543 m. J, *Chatangiella* sp., Zelten Formation; HHH1.2, HHH1 well, 1543 m. K, AOM (blue arrow), opaque matter (green arrow) and *Pediastrum* (red arrow), Zelten Formation; HHH1.2, HHH1 well, 1543 m. L, AOM (blue arrow),

phytoclast (green arrow), *Dinogymnium* (red arrow) and opaque matter (green arrow) from the Zelten Formation; HHH1.2, HHH1 well, 1543 m. M, damaged *Andalusiella* sp., Kheir Formation; AA1.2, AA1 well, 1902 m. N, Resin particle surrounded by pale grey AOM, Kheir Formation; AA1.1, AA1 well, 1728 m. O, Microforaminiferal test linings, Kheir Formation; AA1.1, AA1 well, 1728 m. P, AOMA, Kheir Formation; AA1.2, AA1 well, 1902 m.

Fig. 8. Ternary APP kerogen plot of the samples from the wells studied.

Fig. 9. A, Sirte Formation microfacies; bioclastic floatstone association: bivalve fragment (BI), algae (AL), and oyster (OY), 3589 m, AA1 well. B, Sirte Formation microfacies; planktonic foraminiferal wackstone: numerous pelagic foraminifera (PF) and fragment of oyster shell (OY), 2821 m, AA1 well. C, Kalash Formation microfacies; foraminiferal bioclastic packstone: *Nummulites* (NU), 2727 m, AA1 well. D, Farrud Member microfacies; anhydrite dolomite wackstone, 1652 m, QQQ1 well. E, Zelten Formation microfacies; laminated ferruginous sandy shale association, 1543 m, HHH1 well. F, Kheir Formation microfacies; dismicrite association, 1584 m, RRR1 well.

Fig. 10. A, a conceptual model of the sedimentary environment of the Upper Cretaceous succession in Concession 11; **B,** reconstruction of the main sedimentary facies and depositional environments of the Paleocene to Eocene succession in Concession 11.

Table 1. List of the wells studied in the giant oilfields, Concession 11.

Table 2. Results of TOC and Rock-Eval pyrolysis data on cores and cuttings samples from wells in the western Sirte Basin. **TOC**: Total organic carbon, wt %; **S_1**: Free hydrocarbon content, mg HC/g rock; **S_2**: Remaining hydrocarbon generative potential, mg HC/g rock; **S_3**: Carbon dioxide yield, mg CO_2/g rock; **HI**: Hydrogen index = S_2×100/ TOC, mg HC/g TOC; **OI**: Oxygen index =S_3×100/ TOC, mg CO_2/g TOC; **T_{max}**: Temperature at maximum of S_2 peak; **PI**: Production index = $S_1/(S_1+S_2)$.

Table 3. Quantitative distribution of palynofacies particles recorded from the formations studied.

Table 4. Summary of geochemical and palynofacies parameters for the samples studied.

Table 1

Well name	Field	Coordinates		Pay zone	Age	Total depth (m)
		Latitude (N)	Longitude (E)			
QQQ1	Tagrifet	29° 17′ 25″	17° 23′ 52″	Farrud	Paleocene	2892
LLL1	Daba	29° 15′ 10″	17° 26′ 06″	Farrud	Paleocene	3158
RRR45	Ghani	29° 61′ 34″	17° 27′ 14″	Farrud	Paleocene	1920
RRR40	Ghani	28° 59′ 38″	17° 25′ 37″	Farrud	Paleocene	2530
AA1	Abeter	28° 58′ 15″	17° 23′ 31″	Gir (Facha)	Eocene	3826
RRR1	Ghani	28° 57′ 41″	17° 28′ 00″	Farrud	Paleocene	1877
HHH1	Mellugh	28° 51′ 13″	17° 28′ 28″	Gir (Facha)	Eocene	2865
FFF1	Ed Dib	28° 57′ 30″	17° 30′ 10″	Gir (Facha)	Eocene	3145
GG1	Ed Dib	28° 59′ 34″	17° 34′ 08″	Gir (Facha)	Eocene	3349
RRR32	Ghani	29° 00′ 37″	17° 27′ 02″	Farrud	Paleocene	1876
RRR29	Ghani	29° 00′ 23″	17° 27′ 00″	Farrud–Facha	Paleocene–Eocene	1820
RRR28	Ghani	28° 59′ 02″	17° 26′ 56″	Farrud	Paleocene	1832
RRR25	Ghani	28° 59′ 02″	17° 27′ 48″	Farrud	Paleocene	1827
RRR76	Ghani	28° 58′ 36″	17° 28′ 05″	Farrud	Paleocene	1900

Table 2

Well name	Formation	Sample type	Depth (m)	TOC (wt%)	S_1 (mg/g)	S_2 (mg/g)	S_3 (mg/g)	T_{max} (°C)	HI (mg HC/ g TOC)	OI (mg CO_2/ g TOC)	S_1/ TOC	PI	S_1+S_2 (mg/g)
AA1.3	Kalash	Core	2720	0.31	–	–	–	–	–	–	–	–	–
AA1.4	Kalash	Core	2723	0.41	–	–	–	–	–	–	–	–	–
AA1.5	Kalash	Core	2725	0.38	–	–	–	–	–	–	–	–	–
AA1.6	Kalash	Core	2730	0.29	–	–	–	–	–	–	–	–	–
FFF1.1	Kalash	Core	2372	0.58	0.21	1.11	0.76	437	191	130.58	36.08	0.15	1.32
FFF1.2	Kalash	Core	2374	0.37	–	–	–	–	–	–	–	–	–
FFF1.3	Kalash	Core	2375	0.42	–	–	–	–	–	–	–	–	–
FFF1.5	Kalash	Core	2375	0.63	0.16	1.29	0.7	439	204.43	110.93	25.35	0.11	1.45
FFF1.6	Kalash	Core	2377	0.33	–	–	–	–	–	–	–	–	–
FFF1.7	Kalash	Core	2378	0.19	–	–	–	–	–	–	–	–	–
FFF1.8	Kalash	Core	2379	0.31	–	–	–	–	–	–	–	–	–
FFF1.9	Kalash	Core	2380	2.04	0.33	6.96	1.01	440	341.17	49.50	16.17	0.04	7.29
FFF1.10	Kalash	Core	2382	0.47	0.26	1.07	1.12	437	226.69	237.28	55.08	0.19	1.33
QQQ1.1	Sirte	Cuttings	2431–2432	0.57	0.08	0.47	0.56	435	82.89	98.76	14.10	0.14	0.55
GG1.4	Sirte	Cuttings	2658–2661	1.01	0.35	1.22	0.99	435	120.79	98.01	34.65	0.22	1.57
GG1.5	Sirte	Cuttings	2667–2670	1.01	0.30	1.22	1.26	438	122.24	126.25	30.06	0.19	1.52
GG1.7	Sirte	Cuttings	2676–2679	1.70	0.60	2.04	1.04	447	120.00	61.17	35.29	0.22	2.64
GG1.8	Sirte	Cuttings	2719–2721	1.28	0.54	1.4	1.22	436	109.37	95.31	42.18	0.27	1.94

GG1.9	Sirte	Cuttings	2728–2731	1.39	0.57	1.63	1.06	439	117.26	76.25	41.00	0.25	202
GG1.10	Sirte	Cuttings	2746–2749	1.20	0.51	1.66	0.84	437	138.33	70.00	42.50	0.23	2.17
GG1.11	Sirte	Cuttings	2761–2764	1.04	0.32	0.92	1.00	432	88.46	96.15	30.76	0.25	1.24
GG1.12	Sirte	Cuttings	2780–2783	0.89	0.31	0.74	0.99	433	82.95	110.98	34.75	0.29	1.05
HHH1.3	Sirte	Cuttings	2351–2354	1.02	0.48	2.12	0.8	436	207.84	78.43	47.05	0.18	2.6
HHH1.4	Sirte	Cuttings	2362–2365	1.11	0.40	2.44	0.75	438	219.81	67.56	36.03	0.14	2.84
HHH1.5	Sirte	Cuttings	2374–2377	1.36	0.48	2.97	0.84	438	218.38	61.76	35.29	0.13	3.45
HHH1.6	Sirte	Cuttings	2380–2383	1.25	0.51	2.62	0.78	438	209.60	62.40	40.80	0.16	3.13
HHH1.7	Sirte	Cuttings	2386–2389	1.25	0.50	2.55	0.71	438	204.00	56.80	40.00	0.16	3.05
HHH1.8	Sirte	Cuttings	2399–2402	0.89	0.36	1.69	0.76	435	188.40	84.72	40.13	0.17	2.05
AA1.9	Sirte	Cuttings	3630–3633	0.61	0.24	0.65	0.70	430	105.69	113.82	39.02	0.26	0.89
FFF1.11	Sirte	Core	2402	1.15	0.25	3.32	1.05	439	288.69	91.30	21.73	0.07	3.57
RRR40.1	Sirte	Cuttings	2399	1.64	0.30	4.43	0.96	440	270.12	58.53	18.29	0.06	4.73
RRR40.2	Sirte	Cuttings	2402–2405	1.72	0.41	4.73	0.95	439	275.00	55.23	23.83	0.07	5.14
RRR40.3	Sirte	Cuttings	2414–2417	1.43	0.30	3.71	0.73	440	259.44	51.04	20.97	0.07	4.01
RRR40.4	Sirte	Cuttings	2417–2420	1.52	0.34	4.3	0.74	439	282.89	48.68	22.36	0.07	4.64
RRR40.5	Sirte	Cuttings	2429–2432	1.45	0.33	3.82	0.76	440	263.44	52.41	22.75	0.07	4.15
RRR40.6	Sirte	Cuttings	2472–2475	1.14	0.36	2.6	0.63	442	228.07	55.26	31.57	0.12	2.96
RRR40.7	Sirte	Cuttings	2475–2478	1.15	0.27	2.25	0.93	440	195.65	80.86	23.47	0.10	2.52
RRR40.8	Sirte	Cuttings	2511–2515	0.86	0.19	1.23	0.94	439	142.36	108.79	21.99	0.13	1.42
GG1.13	Rachmat	Cuttings	2798–2801	0.91	0.35	0.84	0.8	434	92.71	88.30	38.63	0.29	1.19

GG1.14	Rachmat	Cuttings	2813–2816	1.08	0.44	1.11	0.77	435	102.77	71.29	40.74	0.28	1.55
GG1.15	Rachmat	Cuttings	2822–2825	1.22	0.45	1.40	0.78	436	114.75	63.93	36.88	0.24	1.85
HHH1.9	Rachmat	Cuttings	2411–2414	0.77	0.22	1.00	0.74	435	129.53	95.85	28.49	0.18	1.22
HHH1.10	Rachmat	Cuttings	2432–2435	0.77	0.23	0.83	0.66	433	108.49	86.27	30.06	0.21	1.06
QQQ1.2	Etel	Cuttings	2792–2795	0.62	0.08	0.55	0.62	434	89.28	100.65	12.98	0.12	1.35
QQQ1.3	Etel	Cuttings	2798–2801	0.61	0.09	0.62	0.56	435	100.97	91.20	14.65	0.12	0.71
QQQ1.4	Etel	Cuttings	2804–2807	0.36	0.08	0.31	0.6	431	86.35	167.13	22.28	0.20	0.39
QQQ1.6	Etel	Cuttings	2841–2844	0.52	0.10	0.31	0.85	431	59.84	164.09	19.30	0.24	0.41
QQQ1.7	Etel	Cuttings	2862–2865	0.62	0.10	0.73	0.63	432	118.50	102.27	16.23	0.12	0.83
AA1.10	Etel	Cuttings	3676–3679	0.51	0.19	0.48	0.78	425	94.30	153.24	37.32	0.28	0.67
AA1.12	Etel	Cuttings	3709–3712	0.58	0.16	0.41	0.69	424	71.18	119.79	27.77	0.28	0.57
LLL1.1	Etel	Cuttings	2774–2777	0.53	0.12	0.51	0.82	431	96.77	155.59	22.77	0.19	0.63
LLL1.2	Etel	Cuttings	2822–2825	0.36	–	–	–	–	–	–	–	–	–
LLL1.3	Etel	Cuttings	2853–2856	0.53	0.14	0.57	0.63	437	107.75	119.09	26.46	0.19	0.71
LLL1.5	Etel	Cuttings	2932–2935	0.56	0.16	0.91	0.53	437	163.96	95.49	28.82	0.14	0.07
FFF1.12	Etel	Cuttings	2871–2874	0.86	0.21	0.84	1.12	432	97.67	130.23	24.41	0.20	1.05
FFF1.14	Etel	Cuttings	2938–2941	0.89	0.15	0.92	1.20	438	103.83	135.44	16.93	0.14	1.07

Table 3

Sample no.	Well name	Depth (m)	Age	Rock unit	Facies	% AOM	% Phyto	% Palyno
AA1.1	AA1	1728	Paleocene-Eocene	Kheir Formation	Foraminferal biomicrite	85	14	1
AA1.2	AA1	1902	Paleocene-Eocene	Kheir Formation	Foraminferal biomicrite	79	20	1
HHH1.1	HHH1	1540	Paleocene (Thanetian)	Zelten Formation	Laminated ferruginous sandy shale	52	45	3
HHH1.2	HHH1	1543	Paleocene (Thanetian)	Zelten Formation	Laminated ferruginous sandy shale	48	50	2
GG1.1	GG1	1741	Paleocene (Danian)	Farrud Member	Foraminiferal biomicrite	75	20	5
GG1.2	GG1	1744	Paleocene (Danian)	Farrud Member	Ostracodal biomicrite	60	36	4
GG1.3	GG1	1767	Paleocene (Danian)	Farrud Member	Micritized biodolomite	50	48	2
FFF1.1	FFF1	2372	Upper Cretaceous (Maastrichtian)	Kalash Formation	Pelagic foraminferal biomicrite	62	36	2
FFF1.2	FFF1	2374	Upper Cretaceous (Maastrichtian)	Kalash Formation	Micritic limestone	70	28	2
FFF1.3	FFF1	2375	Upper Cretaceous (Maastrichtian)	Kalash Formation	Micritic limestone	72	25	3
FFF1.4	FFF1	2376	Upper Cretaceous (Maastrichtian)	Kalash Formation	Micritic limestone	76	18	6
FFF1.5	FFF1	2377	Upper Cretaceous (Maastrichtian)	Kalash Formation	Pelagic foraminiferal biomicrite	86	9	5
FFF1.6	FFF1	2377.5	Upper Cretaceous (Maastrichtian)	Kalash Formation	Pelagic foraminiferal biomicrite	70	24	6
FFF1.7	FFF1	2378	Upper Cretaceous (Maastrichtian)	Kalash Formation	Micritic limestone	77	20	3
FFF1.8	FFF1	2379	Upper Cretaceous (Maastrichtian)	Kalash Formation	Pelagic foraminiferal biomicrite	75	21	4
FFF1.9	FFF1	2380	Upper Cretaceous (Maastrichtian)	Kalash Formation	Micritic limestone	80	13	7
FFF1.10	FFF1	2382	Upper Cretaceous (Maastrichtian)	Kalash Formation	Micritic limestone	77	17	6

AA1.3	AA1	2720	Upper Cretaceous (Maastrichtian)	Kalash Formation	Sandy limestone and dolomite	50	48	2
AA1.4	AA1	2723	Upper Cretaceous (Maastrichtian)	Kalash Formation	Micritic limestone	49	50	1
AA1.5	AA1	2725	Upper Cretaceous (Maastrichtian)	Kalash Formation	Pelagic foraminiferal biomicrite	68	30	2
AA1.6	AA1	2730	Upper Cretaceous (Maastrichtian)	Kalash Formation	Micritic limestone	65	33	2
HHH1.3	HHH1	2351–2353	Upper Cretaceous (Campanian)	Sirte Formation	Shale	79	19	2
HHH1.4	HHH1	2362–2365	Upper Cretaceous (Campanian)	Sirte Formation	Shale	60	39	1
HHH1.5	HHH1	2374–2377	Upper Cretaceous (Campanian)	Sirte Formation	Shale	76	22	2
HHH1.6	HHH1	2380–2383	Upper Cretaceous (Campanian)	Sirte Formation	Shale	68	30	2
HHH1.7	HHH1	2386–2389	Upper Cretaceous (Campanian)	Sirte Formation	Shale	71	28	1
HHH1.8	HHH1	2399–2401	Upper Cretaceous (Campanian)	Sirte Formation	Shale	28	70	2
FFF1.11	FFF1	2401	Upper Cretaceous (Campanian)	Sirte Formation	Pelagic foraminiferal argillaceous micrite	88	11	1
RRR40.1	RRR40	2399	Upper Cretaceous (Campanian)	Sirte Formation	Shale	73	23	4
RRR40.2	RRR40	2402–2405	Upper Cretaceous (Campanian)	Sirte Formation	Shale	73	24	3
RRR40.3	RRR40	2414–2417	Upper Cretaceous (Campanian)	Sirte Formation	Shale	74	21	5
RRR40.4	RRR40	2417–2420	Upper Cretaceous (Campanian)	Sirte Formation	Shale	76	22	2
RRR40.5	RRR40	2429–2432	Upper Cretaceous (Campanian)	Sirte Formation	Shale	72	24	4
RRR40.6	RRR40	2472–2475	Upper Cretaceous (Campanian)	Sirte Formation	Shale	75	22	3
RRR40.7	RRR40	2475–2478	Upper Cretaceous (Campanian)	Sirte Formation	Shale	70	29	1
QQQ1.1	QQQ1	2431–2432	Upper Cretaceous (Campanian)	Sirte Formation	Shale	35	61	4
GG1.4	GG1	2658–2661	Upper Cretaceous (Campanian)	Sirte Formation	Shale	85	12	3

GG1.5	GG1	2667–2670	Upper Cretaceous (Campanian)	Sirte Formation	Shale	27	72	1
GG1.6	GG1	2685–2688	Upper Cretaceous (Campanian)	Sirte Formation	Shale	55	43	2
GG1.9	GG1	2706–2709	Upper Cretaceous (Campanian)	Sirte Formation	Shale	29	70	1
GG1.7	GG1	2719–2722	Upper Cretaceous (Campanian)	Sirte Formation	Shale	28	70	2
GG1.8	GG1	2728–2731	Upper Cretaceous (Campanian)	Sirte Formation	Shale	24	75	1
GG1.10	GG1	2746–2749	Upper Cretaceous (Campanian)	Sirte Formation	Shale	38	60	2
GG1.11	GG1	2761–2764	Upper Cretaceous (Campanian)	Sirte Formation	Shale	28	69	3
GG1.12	GG1	2780–2783	Upper Cretaceous (Campanian)	Sirte Formation	Shale	31	67	2
AA1.7	AA1	3582	Upper Cretaceous (Campanian)	Sirte Formation	Laminated calcareous sandy shale	28	70	2
AA1.8	AA1	3589	Upper Cretaceous (Campanian)	Sirte Formation	Laminated sandy mud biomicrite	21	77	2
AA1.9	AA1	3630–3633	Upper Cretaceous (Campanian)	Sirte Formation	Shale	18	80	2
HHH1.9	HHH1	2410–2414	Upper Cretaceous (Coniacian-Santonian)	Rachmat Formation	Shale with thin limestone and dolomite streaks	33	65	2
HHH1.10	HHH1	2432–2435	Upper Cretaceous (Coniacian-Santonian)	Rachmat Formation	Shale with thin limestone and dolomite streaks	31	67	2
GG1.13	GG1	2798–2801	Upper Cretaceous (Coniacian-Santonian)	Rachmat Formation	Shale with thin limestone and dolomite streaks	14	85	1
GG1.14	GG1	2813–2816	Upper Cretaceous (Coniacian-Santonian)	Rachmat Formation	Shale with thin limestone and dolomite streaks	19	80	1
GG1.15	GG1	2822–2825	Upper Cretaceous (Coniacian-Santonian)	Rachmat Formation	Shale with thin limestone and dolomite streaks	20	79	1
GG1.16	GG1	2831–2835	Upper Cretaceous (Coniacian-Santonian)	Rachmat Formation	Shale with thin limestone and dolomite streaks	25	73	2

LLL1.1	LLL1	2774–2777	Upper Cretaceous (Turonian)	Etel Formation	Dolomitic limestone	18	73	9
LLL1.2	LLL1	2822–2825	Upper Cretaceous (Turonian)	Etel Formation	Dolomitic limestone	39	55	6
LLL1.3	LLL1	2853–2856	Upper Cretaceous (Turonian)	Etel Formation	Dolomitic limestone	27	66	7
LLL1.4	LLL1	2889–2892	Upper Cretaceous (Turonian)	Etel Formation	Dolomitic limestone	23	69	8
LLL1.5	LLL1	2932–2935	Upper Cretaceous (Turonian)	Etel Formation	Dolomitic limestone	26	70	4
QQQ1.2	QQQ1	2792–2795	Upper Cretaceous (Turonian)	Etel Formation	Dolomitic limestone	30	65	5
QQQ1.3	QQQ1	2798–2801	Upper Cretaceous (Turonian))	Etel Formation	Dolomitic limestone	31	66	3
QQQ1.4	QQQ1	2804–2807	Upper Cretaceous (Turonian)	Etel Formation	Dolomitic limestone	35	60	5
QQQ1.5	QQQ1	2822–2825	Upper Cretaceous (Turonian)	Etel Formation	Dolomitic limestone	40	55	5
QQQ1.6	QQQ1	2841–2844	Upper Cretaceous (Turonian)	Etel Formation	Dolomitic limestone	32	66	2
QQQ1.7	QQQ1	2862–2865	Upper Cretaceous (Turonian)	Etel Formation	Dolomitic limestone	30	67	3
FFF1.12	FFF1	2871–2874	Upper Cretaceous (Turonian)	Etel Formation	Dolomitic limestone	21	76	3
FFF1.14	FFF1	2938–2941	Upper Cretaceous (Turonian)	Etel Formation	Dolomitic limestone	34	63	3
GG1.17	GG1	3051	Upper Cretaceous (Turonian)	Etel Formation	Dolomitic limestone	31	68	1
AA1.10	AA1	3676–3679	Upper Cretaceous (Turonian)	Etel Formation	Dolomitic limestone	21	78	1
AA1.11	AA1	3697–3700	Upper Cretaceous (Turonian)	Etel Formation	Dolomitic limestone	34	65	1
AA1.12	AA1	3709–3712	Upper Cretaceous (Turonian)	Etel Formation	Dolomitic limestone	28	70	2
AA1.13	AA1	3725–3728	Upper Cretaceous (Turonian)	Etel Formation	Dolomitic limestone	42	55	3
AA1.14	AA1	3731–3734	Upper Cretaceous (Turonian)	Etel Formation	Dolomitic limestone	39	60	1
LLL1.6	LLL1	2996–2999	Upper Cretaceous (Cenomanian)	Bahi Formation	Sandy limestone and dolomite	29	70	1

LLL1.7	LLL1	3017–3020	Upper Cretaceous (Cenomanian)	Bahi Formation	Sandy limestone and dolomite	26	73	1
LLL1.8	LLL1	3033–3036	Upper Cretaceous (Cenomanian)	Bahi Formation	Sandy limestone and dolomite	39	60	1
LLL1.9	LLL1	3036–3039	Upper Cretaceous (Cenomanian)	Bahi Formation	Sandy limestone and dolomite	43	56	1
AA1.15	AA1	3779–3782	Upper Cretaceous (Cenomanian)	Bahi Formation	Sandy limestone and dolomite	26	70	4
AA1.16	AA1	3813–3816	Upper Cretaceous (Cenomanian)	Bahi Formation	Sandy limestone and dolomite	30	68	2
AA1-17	AA1	3819–3822	Upper Cretaceous (Cenomanian)	Bahi Formation	Sandy limestone and dolomite	28	71	1

Table 4

Sample no.	Depth (m)	Formation	Palynofacies data			Organic geochemistry data					Interpreted kerogen type	
			% AOM	% Phyto.	% Palyno.	TOC (wt%)	S_1 (mg/g)	S_2 (mg/g)	T_{max} (°C)	HI (mg/g)	Palynofacies	Rock-Eval
FFF1.1	2372	Kalash	62	36	2	0.58	0.21	1.11	437	190.72	III (Gas-prone)	III (Gas-prone)
FFF1.5	2375	Kalash	86	9	5	0.63	0.16	1.29	439	204.43	II (Oil-prone)	II/III (Mixed)
FFF1.9	2380	Kalash	80	13	7	2.04	0.33	6.96	440	341.17	II (Oil-prone)	II (Oil-prone)
FFF1.10	2382	Kalash	77	17	6	0.47	0.26	1.07	437	226.69	II (Oil-prone)	II/III (Mixed)
HHH1.3	2351–2353	Sirte	79	19	2	1.02	0.48	2.12	436	207.84	II (Oil-prone)	II/III (Mixed)
HHH1.4	2362–2365	Sirte	60	39	1	1.11	0.40	2.44	438	219.81	II (Oil-prone)	II/III (Mixed)
HHH1.5	2374–2377	Sirte	76	22	2	1.36	0.48	2.97	438	218.38	II (Oil-prone)	II/III (Mixed)
HHH1.6	2380–2383	Sirte	68	30	2	1.25	0.51	2.62	438	209.60	II (Oil-prone)	II/III (Mixed)
HHH1.7	2386–2389	Sirte	71	28	1	1.25	0.5	2.55	438	204.00	II (Oil-prone)	II/III (Mixed)
HHH1.8	2399–2401	Sirte	28	70	2	0.89	0.36	1.69	435	188.40	III (Gas-prone)	III (Gas-prone)
RRR40.1	2399	Sirte	73	23	4	1.64	0.30	4.43	440	270.12	II (Oil-prone)	II/III (Mixed)
RRR40.2	2402–2405	Sirte	73	24	3	1.72	0.41	4.73	439	275.00	II (Oil-prone)	II/III (Mixed)
RRR40.3	2414–2417	Sirte	74	21	5	1.43	0.30	3.71	440	259.44	II (Oil-prone)	II/III (Mixed)
RRR40.4	2417–2420	Sirte	76	22	2	1.52	0.34	4.30	439	282.89	II (Oil-prone)	II/III (Mixed)
RRR40.5	2429–2432	Sirte	72	24	4	1.45	0.33	3.82	440	263.44	II (Oil-prone)	II/III (Mixed)
RRR40.6	2472–2475	Sirte	75	22	3	1.14	0.36	2.60	442	228.07	II (Oil-prone)	II/III (Mixed)
RRR40.7	2475–2478	Sirte	68	31	1	1.15	0.27	2.25	440	195.65	II (Oil-prone)	III (Gas-prone)
QQQ1.1	2431–2434	Sirte	35	61	4	0.56	0.08	0.47	435	82.89	III (Gas-prone)	III (Gas-prone)
GG1.4	2658–2661	Sirte	85	12	3	1.01	0.35	1.22	435	120.79	II (Oil-prone)	III (Gas-prone)
GG1.5	2667–2670	Sirte	27	72	1	0.99	0.30	1.22	438	122.24	III (Gas-prone)	III (Gas-prone)
GG1.7	2685–2688	Sirte	28	70	2	1.70	0.60	2.04	447	120.00	III (Gas-prone)	III (Gas-prone)
GG1.8	2706–2709	Sirte	24	75	1	1.28	0.54	1.40	436	109.37	III (Gas-prone)	III (Gas-prone)
GG1.9	2719–2722	Sirte	29	70	1	1.39	0.57	1.63	439	117.26	III (Gas-prone)	III (Gas-prone)
GG1.10	2728–2731	Sirte	38	60	2	1.20	0.51	1.66	437	138.33	III (Gas-prone)	III (Gas-prone)
GG1.11	2746–2749	Sirte	28	69	3	1.04	0.32	0.92	432	88.46	III (Gas-prone)	III (Gas-prone)
GG1.12	2761–2764	Sirte	31	67	2	0.89	0.31	0.74	433	82.95	III (Gas-prone)	III (Gas-prone)
FFF1.11	2401	Sirte	88	11	1	1.15	0.25	3.32	439	288.69	II (Oil-prone)	II/III (Mixed)

AA1.9	3630–3633	Sirte	18	80	2	0.61	0.24	0.65	430	105.69	III (Gas-prone)	III (Gas-prone)
HHH1.9	2411–2414	Rachmat	33	65	2	0.77	0.22	1.00	435	129.53	III (Gas-prone)	III (Gas-prone)
HHH1.10	2432-2435	Rachmat	31	67	2	0.76	0.23	0.83	433	108.49	III (Gas -prone)	III (Gas-prone)
GG1.13	2798–2801	Rachmat	14	85	1	0.90	0.35	0.84	434	92.71	III (Gas-prone)	III (Gas-prone)
GG1.14	2813–2816	Rachmat	19	80	1	1.08	0.44	1.11	435	102.77	III (Gas-prone)	III (Gas-prone)
GG1.15	2822–2825	Rachmat	20	79	1	1.22	0.45	1.40	436	114.75	III (Gas-prone)	III (Gas-prone)
QQQ1.2	2792–2795	Etel	30	65	5	0.61	0.08	0.55	434	89.28	III (Gas-prone)	III (Gas-prone)
QQQ1.3	2798–2801	Etel	31	66	3	0.61	0.09	0.62	435	100.97	III (Gas-prone)	III (Gas-prone)
QQQ1.4	2804–2807	Etel	35	60	5	0.35	0.08	0.31	431	86.35	III (Gas-prone)	III (Gas-prone)
QQQ1.6	2822–2825	Etel	32	66	2	0.51	0.10	0.31	431	59.84	III (Gas-prone)	III (Gas-prone)
QQQ1.7	2841–2844	Etel	30	67	3	0.61	0.10	0.73	432	118.50	III (Gas-prone)	III (Gas-prone)
FFF1.12	2871–2874	Etel	21	76	3	0.86	0.21	0.84	432	97.67	III (Gas-prone)	III (Gas-prone)
FFF1.14	2938–2941	Etel	34	63	3	0.88	0.15	0.92	438	103.83	III (Gas-prone)	III (Gas-prone)
AA1.10	3676–3679	Etel	21	78	1	0.50	0.19	0.48	425	94.30	III (Gas-prone)	III (Gas-prone)
AA1.12	3709–3712	Etel	28	70	2	0.57	0.16	0.41	424	71.18	III (Gas-prone)	III (Gas-prone)
LLL1.1	2774–2777	Etel	18	73	9	0.52	0.12	0.51	431	96.77	III (Gas-prone)	III (Gas-prone)
LLL1.3	2853–2856	Etel	27	66	7	0.52	0.14	0.57	437	107.75	III (Gas-prone)	III (Gas-prone)
LLL1.5	2932–2935	Etel	26	70	4	0.55	0.16	0.91	437	163.96	III (Gas-prone)	III (Gas-prone)

Figure 1

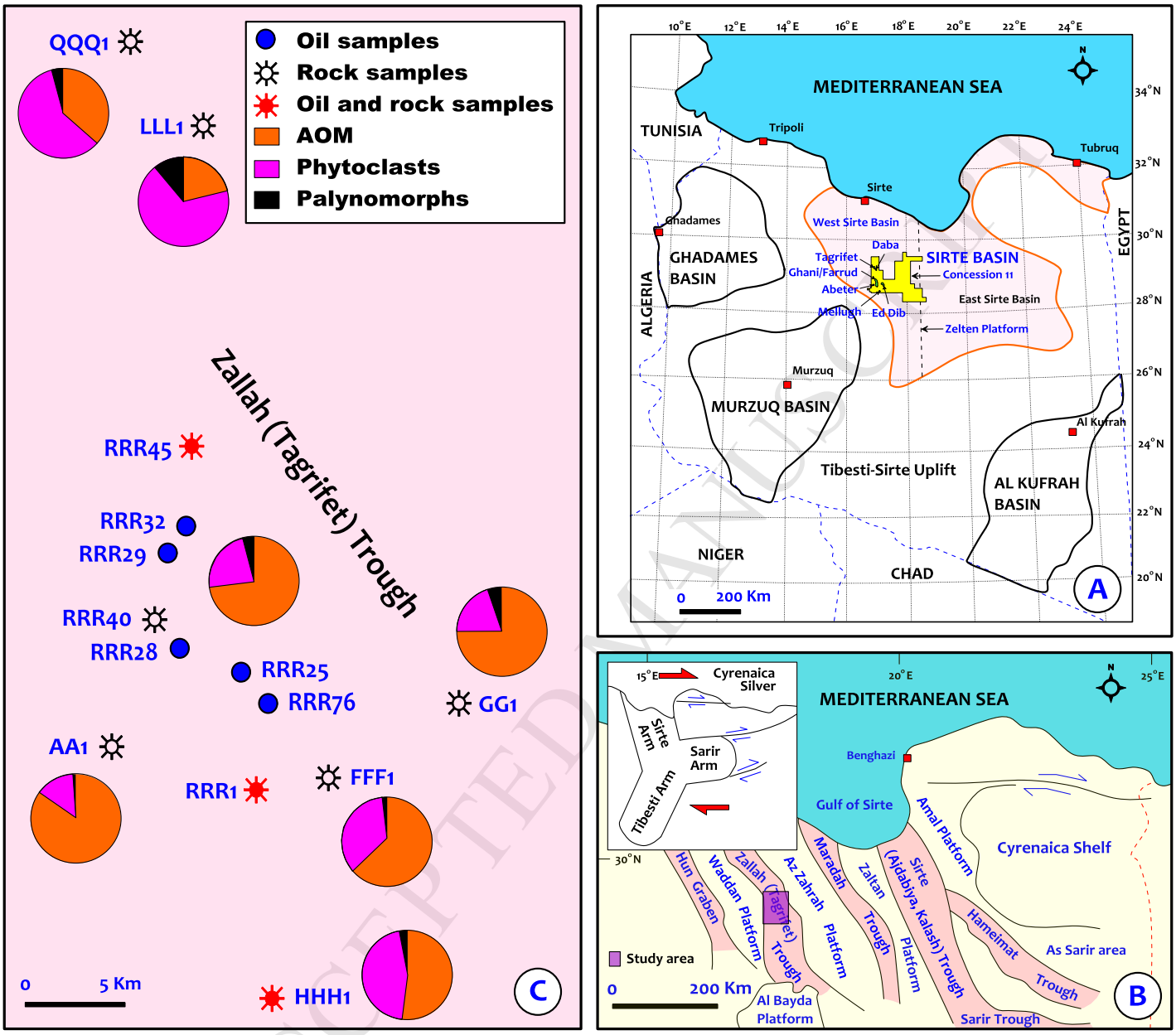

Figure 2

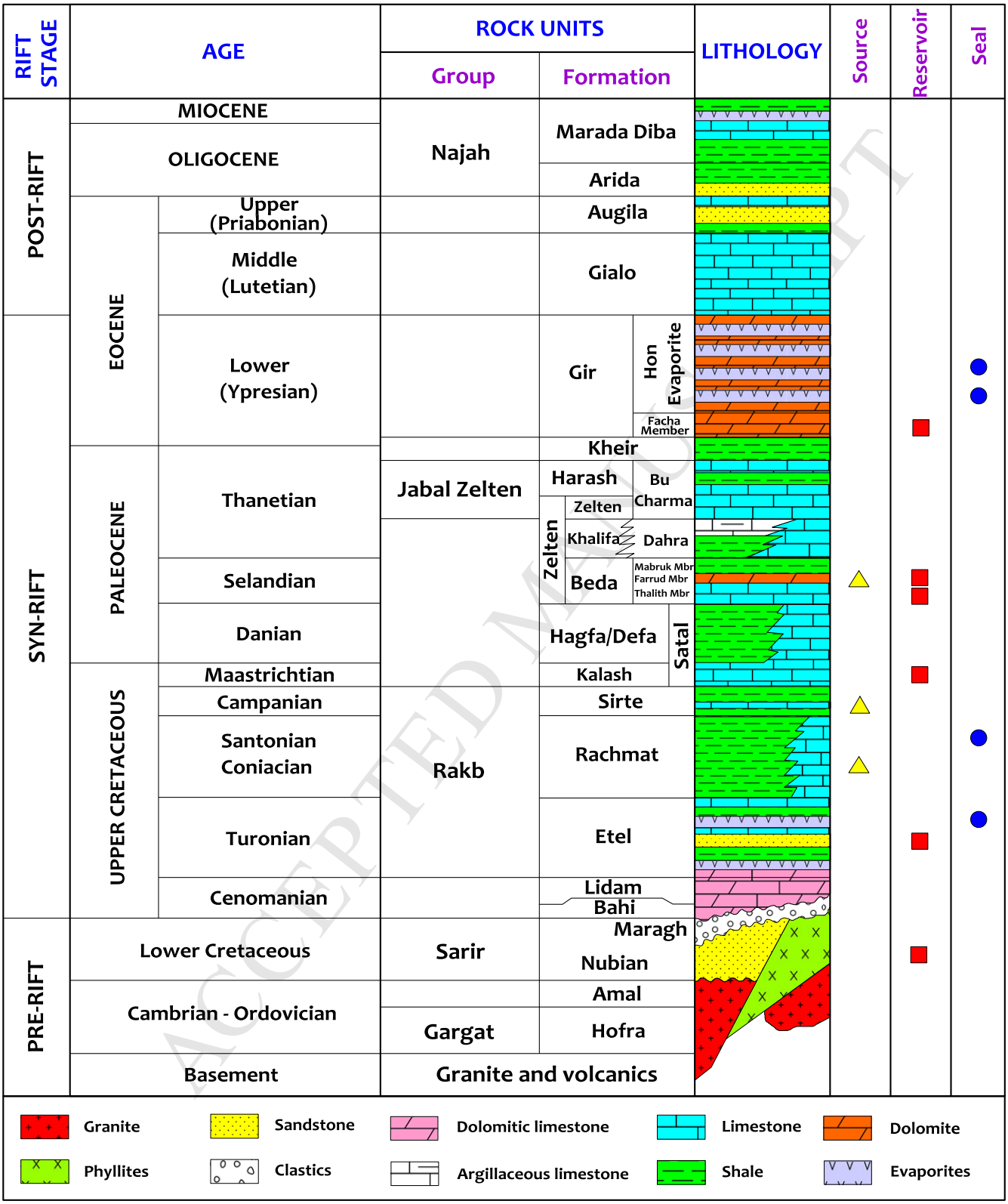

Figure 3

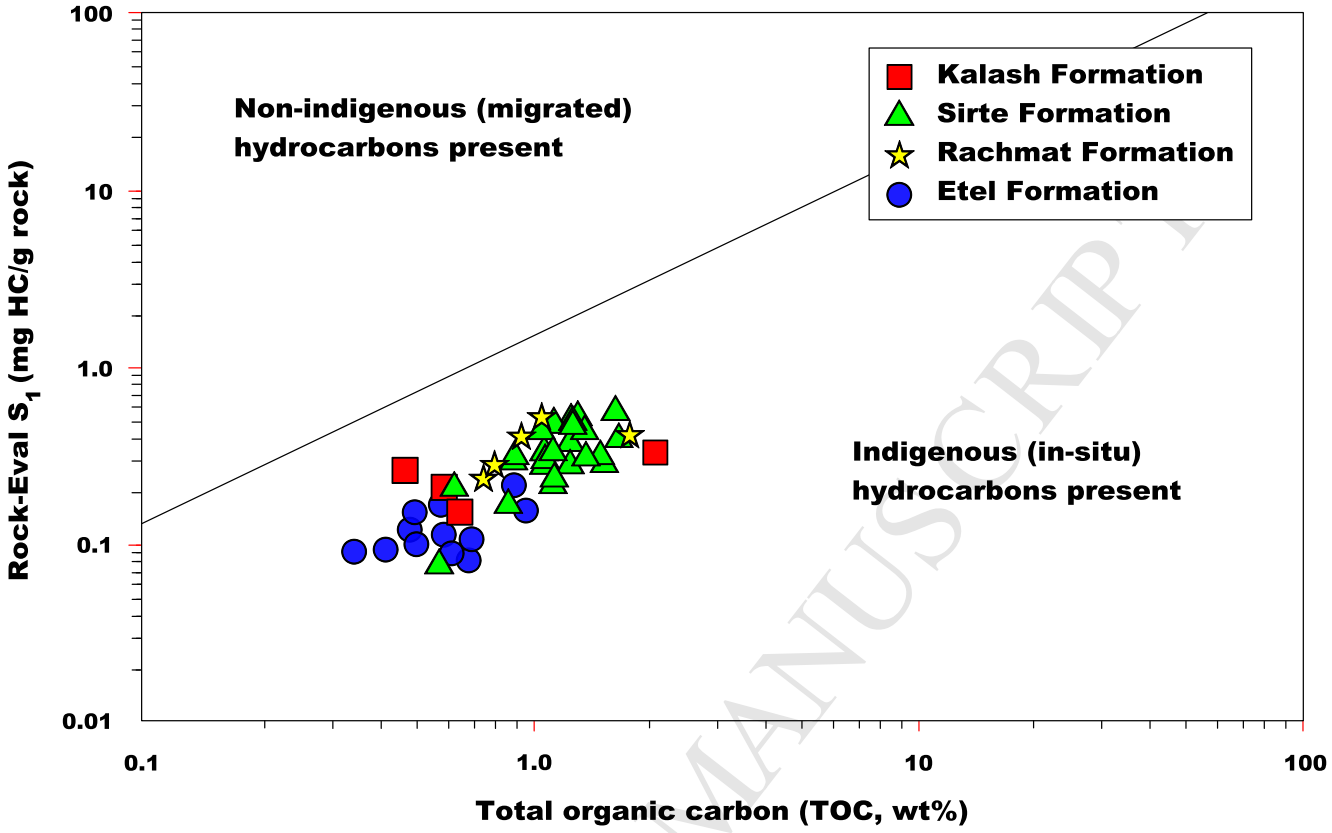

Figure 4

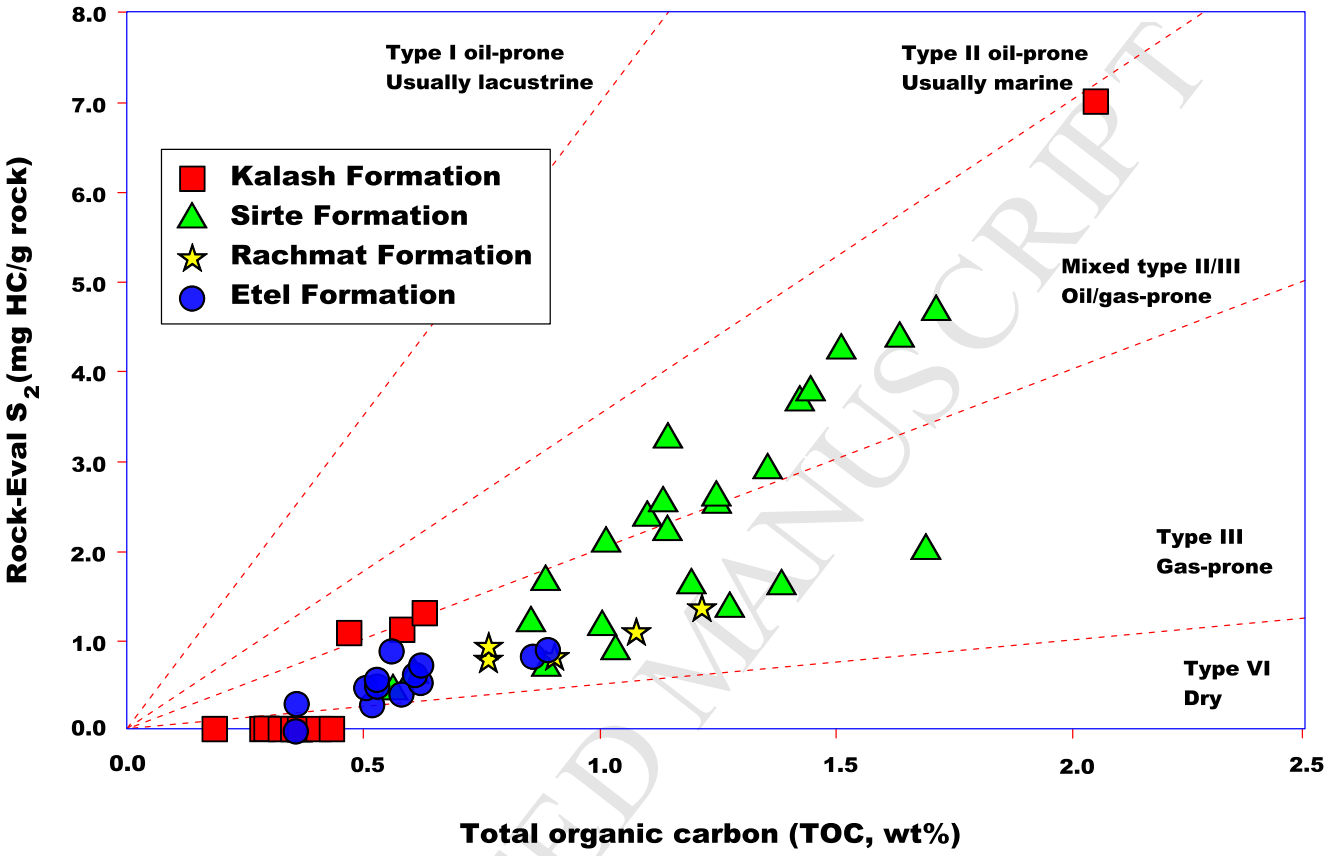

Figure 5

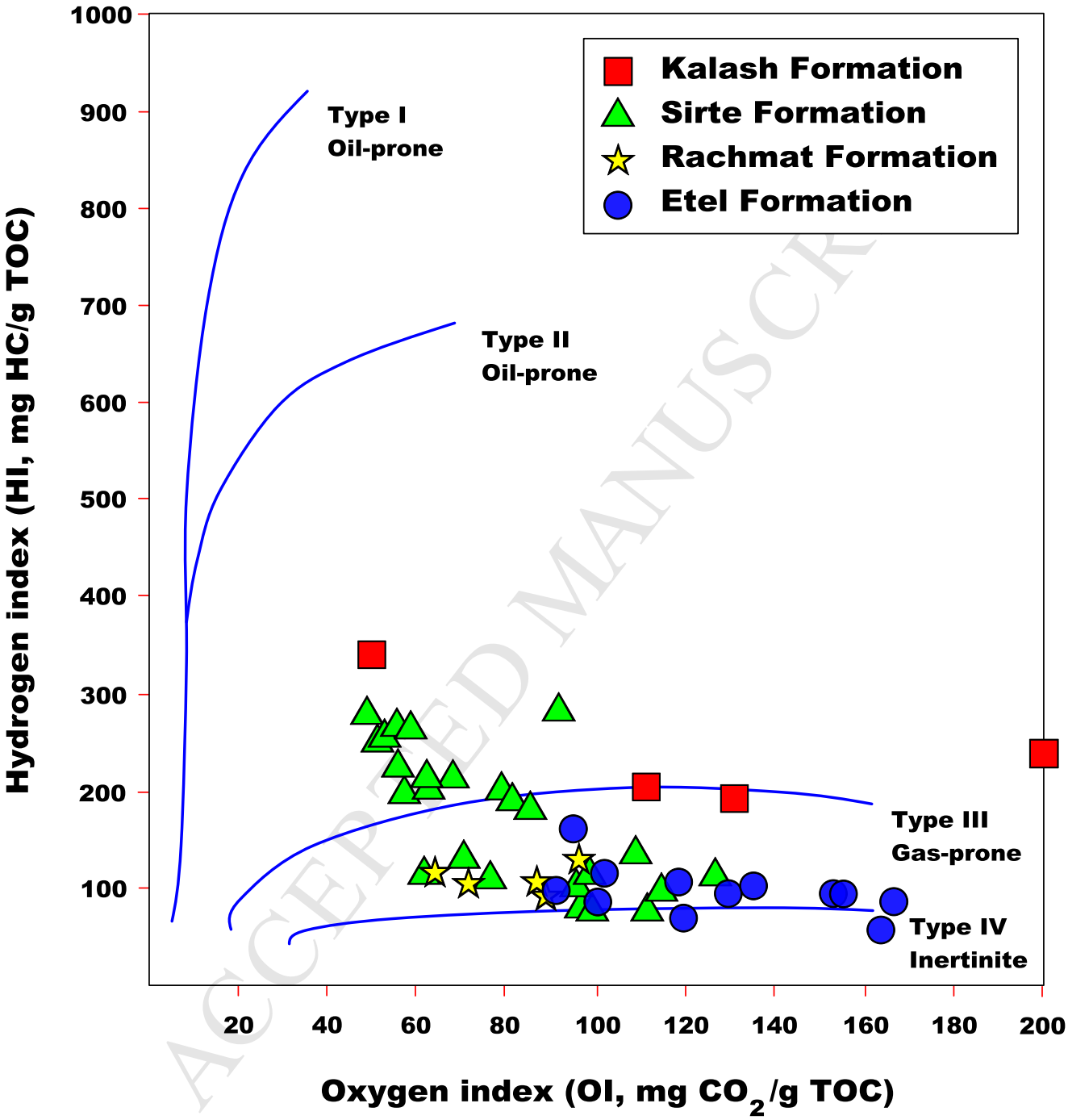

Figure 6

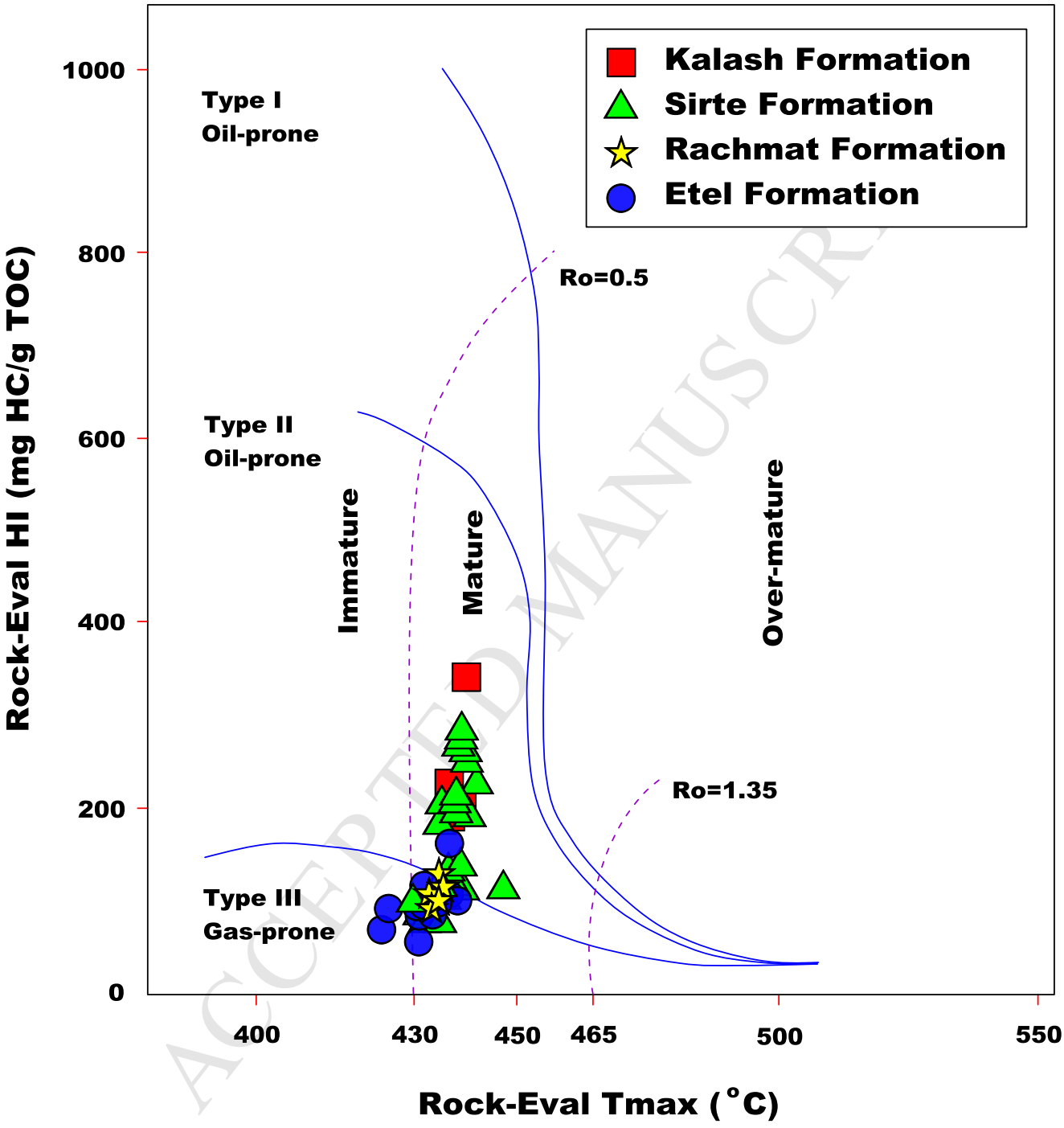

Figure 7

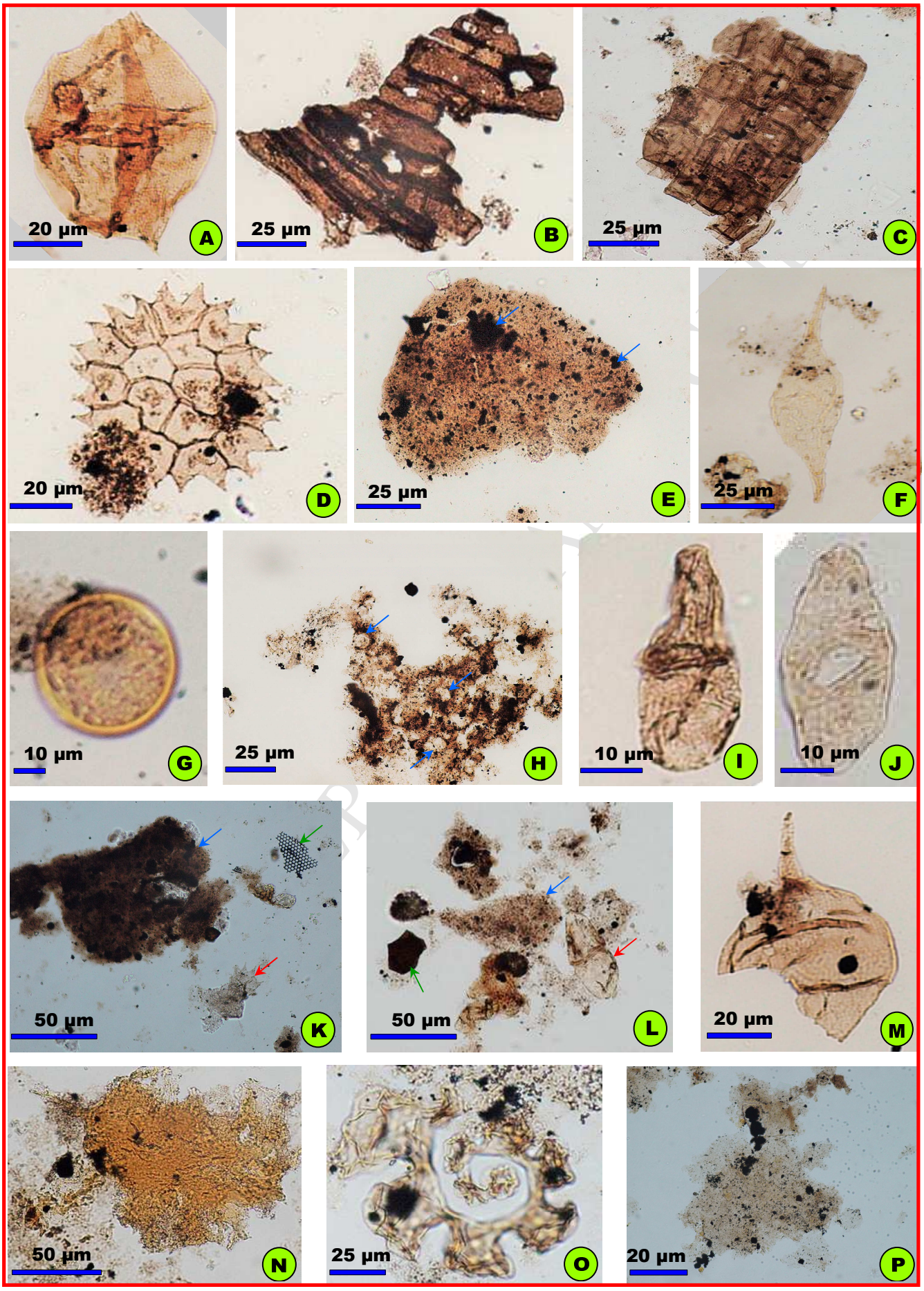
20 µm
A
25 µm
B
25 µm
C
20 µm
D
25 µm
E
25 µm
F
10 µm
G
25 µm
H
10 µm
I
10 µm
J
50 µm
K
50 µm
L
20 µm
M
50 µm
N
25 µm
O
20 µm
P

Figure 8

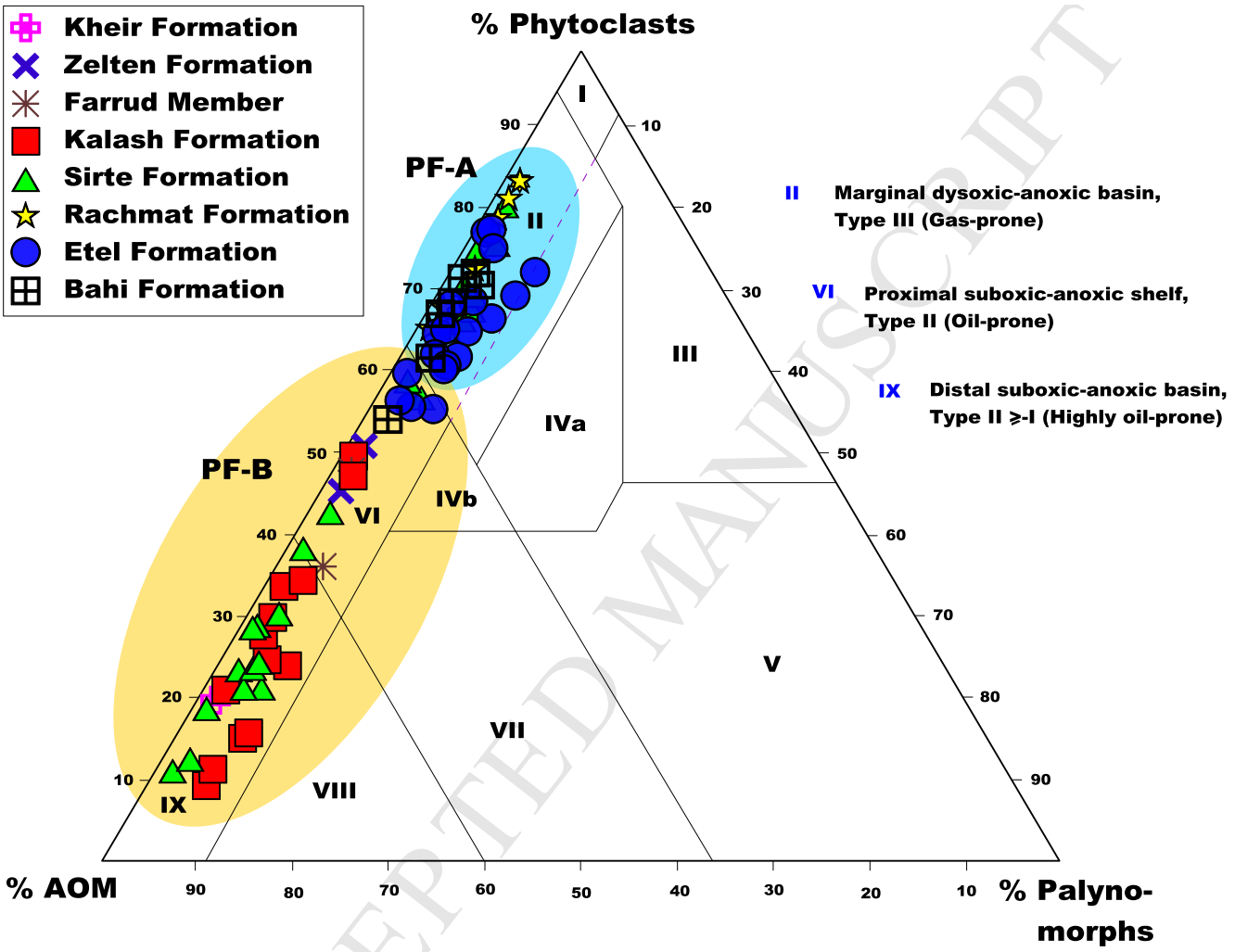

Figure 9

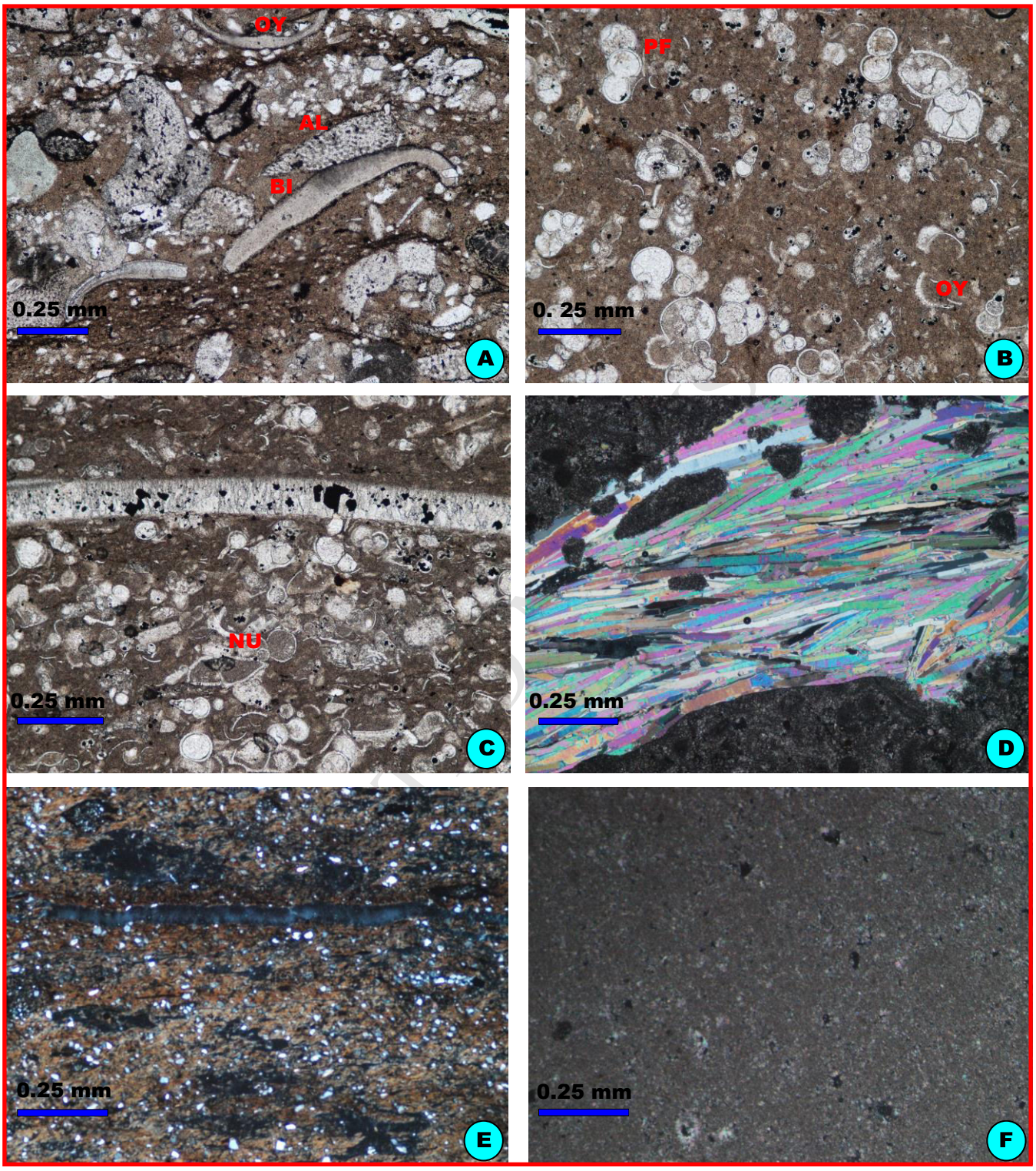

Figure 10

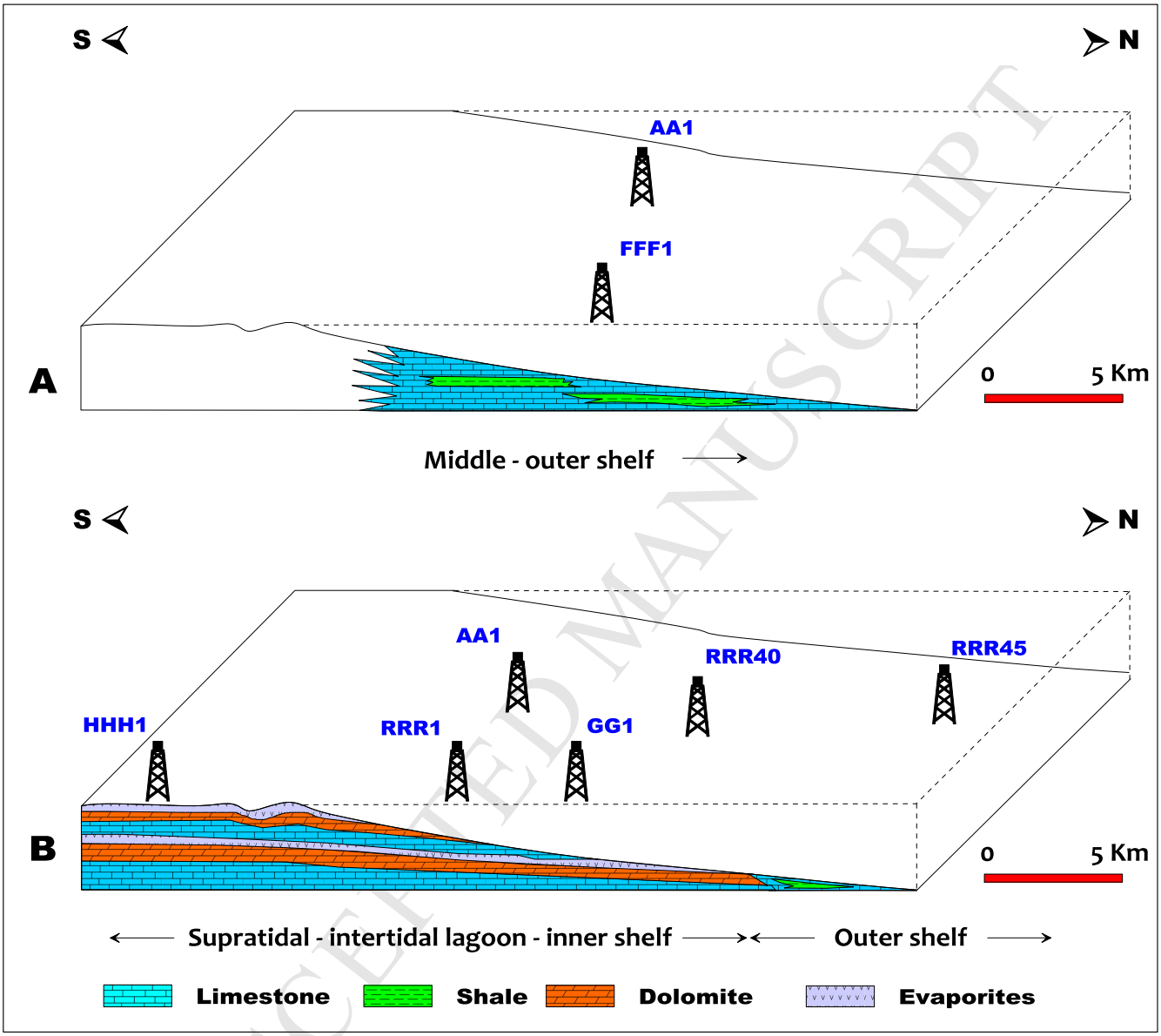

Highlights

- Upper Cretaceous–Eocene rocks, western Sirte Basin, sea levels and tectonic activity
- Facies, palaeoenvironments, source potential for hydrocarbons
- The Cretaceous samples contain mostly moderate amounts of Types-II and II/III kerogen
- Geochemical and palynofacies data reflect deposition mainly in reducing, suboxic settings
- Both immature to early mature gas-prone and mature oil/gas-prone source rocks recorded